

Modeling Rapidly Varied Flow in Tailwaters

MICHAEL G. FERRICK

U.S. Army Cold Regions Research and Engineering Laboratory

JONATHAN BILMES

General Digital Corporation

SAM E. LONG

TVA Water Systems Development Branch

An understanding of the downstream propagation of sharp-fronted, large-amplitude waves of relatively short period is important for describing rapidly varying flows in tailwaters of hydroelectric plants and following the breach of a dam. We developed a numerical model of these waves by first identifying the primary physical processes and then performing an analysis of the solution. A linear analysis of the dynamic open channel flow equations provides relationships describing flow wave advection, diffusion, and dispersion in rivers. A one-dimensional diffusion wave model modified for application to tailwaters simulates the important physical processes and is straightforward to apply. The "modified equation" and von Neumann analyses provide insight into the effects of numerical parameters θ , Δx , and Δt upon stability and dissipative and dispersive behavior of the solution, but the Hirt analysis is found to yield incorrect phase relationships. The capability and accuracy of the model are enhanced when physical diffusion of a river wave is balanced by numerical diffusion in the model. Field studies were conducted in two greatly different tailwaters to assess our understanding of large-scale, rapidly varying flow waves. The accurate simulation of waves having wide-ranging amplitudes, shapes, periods, and base flows attests to the soundness of both the physical basis of the model and the numerical solution technique. These studies reveal that diffusion of short-period waves in natural, free-flowing rivers is significant and that inertia is negligible.

INTRODUCTION

Current concerns regarding energy resources have renewed interest in hydroelectric power generation, particularly for meeting peak power demands. Peak power generation with hydropower creates flow regimes in tailwater rivers characterized by high and low flows, with abrupt flow and stage transitions between these states. Because of these abnormal flow conditions, water temperature and quality in tailwaters are modified from those occurring naturally in the stream. Lengthy periods of zero flow resulting from low power demand or water availability affect the ability of a tailwater to maintain a viable aquatic ecosystem. Sharp stage transitions in winter can disrupt a stable ice cover, inducing ice jamming and frazil ice generation. Therefore, an accurate description of the rapidly varying flow regime is important to assess potential effects of peak power generation upon a stream. In addition, understanding these downstream-propagating, sharp-fronted, large-amplitude flow waves of relatively short period is important because of similarity to waves following the breach of a dam.

In this paper we will develop a numerical model to investigate the flow regime of a tailwater by first determining the physical processes of primary importance and then analyzing the numerical solution technique. Analysis of the physical processes was undertaken because flow regimes in tailwaters are complex, and general mathematical descriptions are burdensome and do not necessarily provide the most useful and accu-

rate model. Though frequently given little attention, analysis of the numerical solution is critical to understanding model behavior and thus for optimal selection of numerical parameters and interpretation of model output.

Analysis of the dynamic open-channel flow equations yields insight into the physical processes of importance in tailwater flow. The processes of wave advection, diffusion, and dispersion in channels are related to terms in the momentum equation. Presented in nondimensional form, the relative magnitudes of these processes indicate the importance of terms in the momentum equation and provide physical insights that guide model selection. This analysis indicates that relatively short-period waves in rivers are significantly affected by diffusion and that inertia has a small effect upon flow waves at relatively small Froude numbers in natural channels, contradicting the general belief that inertia is important in rapidly varying flows. Therefore, we selected and modified the inertia-free diffusion wave model of Koussis [1976] for application to tailwater flow.

Exact solutions of the continuity equation that forms the basis of the diffusion wave model do not exhibit diffusion that is necessary to simulate wave movement in natural rivers. Through analysis of the numerical solution, however, it is possible to compensate for the lack of physical diffusion by quantifying and controlling numerical diffusion. Also, the analysis of the model guides numerical mesh selection (Δx , Δt) for optimal accuracy. The analysis of a numerical model is basic to model development but is frequently limited to the development of stability criteria. Numerical stability requires that errors introduced in the solution do not increase in magnitude as the computation progresses. Numerical models must be stable if the solution obtained is to be meaningful. The con-

Copyright 1984 by the American Geophysical Union.

Paper number 3W1757.
0043-1397/84/003W-1757\$05.00

ditions required for stability of many numerical schemes are known, and numerical instability is generally apparent. The von Neumann and Hirt analyses are frequently used to develop stability criteria [Roache, 1976].

Numerical solutions of the unsteady open channel flow equations typically exhibit errors in both amplitude and phase that may not be apparent without further analysis. Numerical dissipation or diffusion causes the Fourier components of the solution and the errors to be damped. Numerical dispersion results when the modeled wave celerity of some wavelength components differ from those of the governing equation, improperly modifying the wave form as the computation proceeds. The effects of numerical dissipation and dispersion upon the solution are subtle but gradually destroy the correspondence between model and prototype. An improved understanding of the dissipative and dispersive behavior of the numerical model enables the analyst to minimize or exploit these effects to enhance model accuracy and to better interpret computed results.

Though only strictly applicable to linear equations, the "modified equation" [Warming and Hyett, 1974], Hirt and von Neumann analyses are used to relate the dissipative and dispersive behavior of the model to parameters of the numerical solution. A set of linear routings is used to demonstrate the model behavior predicted with the analysis and to verify the adequacy of an expression for numerical diffusion developed in the modified equation analysis.

We compare model simulations with extensive field data from a number of large-amplitude, sharp-fronted waves in the Apalachia and Norris Dam tailwaters that have very different bed slope and roughness characteristics. The accuracy achieved with the model in these field applications verifies its generality for rapidly varying river flow and reinforces the utility of both the analysis of the dynamic equations and the analysis of numerical solution behavior. The field applications demonstrate the importance of flow wave diffusion and the dominance of friction over inertia in rivers.

PHYSICAL BASIS FOR MODEL DEVELOPMENT

The development of a mathematical statement describing important unsteady flow processes in a specific case relies upon a clear physical understanding. In this section we will develop a framework for obtaining insights into flow wave movement in open channels from the one-dimensional dynamic equations. The dynamic equations of flow in open channels (St. Venant equations) are the commonly used statements of conservation of mass and momentum balance when the longitudinal is the important spatial dimension. Flow in unstratified or weakly stratified reservoirs and in rivers having a significant base flow is generally modeled by using these equations; however, standard numerical solutions fail if the flow depth approaches zero. This condition is common in tailwaters of dams used to generate peak power, motivating the search for an alternate mathematical statement. If the local and advective inertia terms of the momentum equation are neglected, the resulting equations can be solved without difficulty as the flow depth becomes small. However, Cunge *et al.* [1980] caution that routing methods based upon inertia-free equations may not be applicable in situations where rapid stage and discharge variations occur, such as in tailwaters.

The dynamic equations for a free-flowing river with a wide prismatic rectangular channel and no local inflow are

$$\frac{\partial y}{\partial t} + \frac{1}{B} \frac{\partial Q}{\partial x} = 0 \quad (1)$$

$$\frac{1}{g} \frac{\partial Q}{\partial t} + \frac{2Q}{gBy} \frac{\partial Q}{\partial x} + \left(By - \frac{Q^2}{gBy^2} \right) \frac{\partial y}{\partial x} - ByS_0 + \frac{1}{C^2B} \left(\frac{Q}{y} \right)^2 = 0 \quad (2)$$

where t is time (s), x is distance along the channel (m), y is flow depth (m), Q is discharge (m^3/s), B is channel width (m), g is acceleration due to gravity (m/s^2), S_0 is the slope of the channel bottom, and C is the Chezy conveyance coefficient ($\text{m}^{1/2}/\text{s}$). If the coefficients of (1) and (2) are assumed constant at appropriate reference values, the equations can be combined and expressed in terms of a single dependent variable yielding

$$\frac{\partial Q}{\partial t} + \left[\frac{3Q}{2By} \right] \frac{\partial Q}{\partial x} + \left[\frac{Q^3 - gB^2y^3S_0}{2gB^3y^3S_0} \right] \frac{\partial^2 Q}{\partial x^2} + \left[\frac{Q^2}{gB^2y^2S_0} \right] \frac{\partial^2 Q}{\partial x \partial t} + \left[\frac{Q}{2gByS_0} \right] \frac{\partial^2 Q}{\partial t^2} = 0 \quad (3)$$

a hyperbolic equation. Equation (3) can be manipulated further to eliminate the second-order mixed and temporal derivatives

$$\frac{\partial Q}{\partial t} + c \frac{\partial Q}{\partial x} = D \frac{\partial^2 Q}{\partial x^2} + E \frac{\partial^3 Q}{\partial x^3} + (\text{higher-order terms})$$

$$c = \frac{3Q}{2By} = \frac{dQ}{dA} \quad (4)$$

$$D = \frac{Q}{2BS_0} (1 - F^2/4)$$

$$E = \frac{Q^2}{2gB^2y^2S_0} D = F^2 \frac{y}{2S_0} D$$

where c is wave celerity, A the channel cross-sectional area, and F the Froude number V/\sqrt{gy} . If second- and higher-order terms in (4) are neglected, the kinematic wave equation, free of physically based diffusion, is obtained. When third- and higher-order terms are neglected, (4) contains positive physical diffusion, and describes a diffusion wave.

The wave celerity given in (4) is that of a kinematic wave and is a consequence of the importance of friction in river flow. The kinematic wave celerity is typically much slower than the dynamic wave celerity $V + \sqrt{gy}$, important when friction is small in relation to inertia. Tracing through the development of (4) reveals that the source of the diffusion term is primarily the water surface slope term of the momentum equation. The dependence of the diffusion coefficient D upon the Froude number results from including the inertia terms in the development. The dispersion coefficient E , given in (4), varies linearly with the magnitude of the diffusion coefficient and quadratically with the Froude number. The existence of the dispersion term and the higher-order terms follow from the inertia terms. When the Froude number is significantly less than 1, (4) simplifies to the advective diffusion equation developed by Cunge [1969], neglecting inertia.

The opposing tendencies of wave diffusion and wave steepening due to nonlinear advection are combined in (4). Whitham [1974] studied the wave front separating steady flow domains with a simplified form of (4) having constant D and excluding terms higher than second order. He found that a steady transition profile evolves and remains continuous when diffusion is present that has a length proportional to the magnitude of D . The magnitude of D approaches zero for smooth, steep channels, which therefore are good candidates for shock

formation and successful application of the kinematic wave equation.

With reference discharge Q_0 and spatial and temporal increments Δx and Δt , (4) is rewritten in dimensionless form in terms of $Q^* = Q/Q_0$, $x^* = x/\Delta x$, and $t^* = t/\Delta t$ as

$$\frac{\partial Q^*}{\partial t^*} + C_r \frac{\partial Q^*}{\partial x^*} = D^* C_r \frac{\partial^2 Q^*}{\partial x^{*2}} + E^* D^* C_r \frac{\partial^3 Q^*}{\partial x^{*3}} + (\text{higher-order terms})$$

$$C_r = \frac{c\Delta t}{\Delta x} \tag{5}$$

$$D^* = \frac{D}{c\Delta x}$$

$$E^* = \frac{Q^2}{2gB^2y^2S_0\Delta x} = F^2 \left(\frac{y}{2S_0\Delta x} \right)$$

where C_r is the Courant number, D^* a dimensionless diffusion coefficient, and E^* a dimensionless dispersion coefficient. The magnitude of Δx selected should provide adequate resolution of the features of the shortest wavelength of interest.

The magnitude of D^* relative to 1 is a measure of the importance of diffusion relative to advection. When this quantity is significantly less than 1, advection is dominant over diffusion. The magnitude of E^* relative to 1 measures the importance of dispersion relative to diffusion. As E^* is proportional to the square of the Froude number, its magnitude for natural rivers is generally much less than 1, revealing that the flow is dominated by friction and essentially independent of inertia.

The validity of using inertia-free methods for rapidly varying tailwater flow can be investigated further with the framework provided by the linear small perturbation analyses of Ponce and Simons [1977], Ponce et al. [1978], and Menéndez and Norscini [1982] and the order-of-magnitude analysis of Henderson [1963]. The results of Ponce et al. can be readily used to gain insight into attenuation and propagation characteristics of the inertia-free models relative to those of the dynamic model. For a range of channel and flow parameters characteristic of tailwaters, attenuation and propagation errors resulting from neglecting inertia appear small. Henderson compared terms of the momentum equation for a wide rectangular channel and found that the inertia terms were of the same order of magnitude and were related to the water surface slope term as

$$\frac{\text{inertia term}}{\partial y/\partial x} = O(F^2) \tag{6}$$

This result supports the relationship between inertia and the square of the Froude number given in (4). Henderson also compared the water surface and bottom slope terms, obtaining

$$\frac{\partial y/\partial x}{S_0} \propto \frac{\partial q/\partial t}{q^{2/3}S_0^{5/3}}$$

where q is the discharge per unit width. For flood flows in natural streams the magnitude of the water surface slope is often small in relation to that of the bottom slope. However, in tailwaters where sudden large-magnitude flow changes occur, $\partial q/\partial t$ can be large, and the water surface slope is expected to make an important contribution to the momentum balance. The importance of the water surface slope is enhanced further in rivers having small bottom slopes.

The analyses support the use of an inertia-free model for

tailwater flow and indicate the importance of diffusion resulting from the water surface slope. The water surface slope is discontinuous at the toe of a rapidly varying flow wave, and a number of waves may exist simultaneously in a tailwater, introducing additional modeling complications of accurately locating each front and evaluating the water surface slope in the vicinity of a front. The kinematic wave equation neglects the water surface slope term in addition to the acceleration terms of the momentum equation, avoiding these complications. This additional simplification does not permit wave diffusion; however, numerical solutions of the kinematic wave equation frequently exhibit diffusion resulting from the solution technique [Cunge, 1969; Smith, 1980]. If this numerical diffusion is used to mimic the physical diffusion occurring in the channel, the inherent model limitation to diffusion-free flows can be overcome.

As a physically meaningful downstream boundary is not generally available in tailwaters, models not requiring a downstream boundary condition are most readily applied. Solutions of the kinematic wave equation are independent of downstream influences and do not require a downstream boundary condition. This model cannot account for the influence of downstream controls upon the flow, and application to rivers with long pooled reaches is suspect. However, Smith [1980] found that a variable weighting factor in the numerical scheme, corresponding to a variable diffusion coefficient, allowed successful application of kinematic wave-based models to flood routing through flat, ponded reaches. The importance of backwater effects upon rapidly varying flows found in tailwaters has not been resolved.

DESCRIPTION OF THE DIFFUSION WAVE FLOW ROUTING MODEL

Our diffusion wave model for flow in tailwaters differs from most kinematic wave routing methods [Weinmann and Laurenson, 1979] in that both stage and discharge are computed at each point in the numerical grid. The conservation of mass equation is solved numerically for discharge. Exact solutions of the continuity equation do not exhibit diffusion, which is necessary to represent important physical processes in tailwater flows. The numerical solution of this equation, however, is adjusted in the model to require numerical diffusion to mimic physical diffusion. The equation for river stage includes a water surface slope term that generates a looped rating curve and provides an improved estimate of wave celerity. The equations are coupled through the wave celerity and must be solved simultaneously.

The continuity equation for flow in open channels can be written as

$$\frac{\partial Q}{\partial x} + \frac{1}{c} \frac{\partial Q}{\partial t} = q_i$$

$$c = \frac{dQ}{dA} = \frac{dx}{dt} \tag{7}$$

where q_i is local inflow per unit length of the channel. Equation (7), which forms the basis of the model, is a first-order hyperbolic equation. This equation type is advantageous for modeling tailwater flow because a downstream boundary condition need not be specified, but for this same reason, backwater effects cannot be taken into account.

The "method of lines," in which the spatial derivative is approximated with a finite difference expression but the dependent variable remains continuous in time, is used to obtain a solution of (7). The partial differential equation for conser-

vation of mass is thereby reduced to an ordinary differential equation. With the approximations

$$\frac{\partial Q}{\partial x} \approx \frac{1}{\Delta x} [Q_{j+1}(t) - Q_j(t)] \quad (8)$$

$$\frac{\partial Q}{\partial t} \approx \theta \frac{\partial Q_j}{\partial t} + (1 - \theta) \frac{\partial Q_{j+1}}{\partial t} \quad (9)$$

in which j is an index corresponding to the spatial location $x = j\Delta x$, and θ is a parameter of the numerical solution, (7) is rewritten as

$$\dot{Q}_{j+1}(t) + aQ_{j+1}(t) = aQ_j(t) + a\Delta x q(t) - \frac{\theta}{(1-\theta)} \dot{Q}_j(t) \quad (10)$$

where

$$a = \frac{\langle \bar{c} \rangle}{\Delta x(1-\theta)}$$

\dot{Q} is the derivative of discharge with respect to time, and $\langle \bar{c} \rangle$ is an averaged celerity in space and time over the cell of the computational mesh where the equation is applied. Assuming, for a small time increment, that the variation of $Q_j(t)$ is linear, that the values of the coefficients can be estimated, and that the local inflow is constant, the solution of (10) is

$$Q_{j+1}^{m+1} = (1-\alpha)Q_j^{m+1} + (\alpha-\beta)Q_j^m + \beta Q_{j+1}^m + q\Delta x(1-\beta) \quad (11)$$

where

$$\beta = \exp\left(\frac{-C_r}{1-\theta}\right)$$

$$\alpha = \frac{1-\beta}{C_r}$$

$$C_r = \frac{\langle \bar{c} \rangle \Delta t}{\Delta x}$$

The local Courant number of the numerical grid cell C_r expresses the ratio of physical to numerical wave celerity, and m is the temporal index of the computational grid $t = m\Delta t$.

Neglecting the inertia of the flow and the momentum contribution of the local inflow, the momentum equation for prismatic channels is

$$\frac{\partial y}{\partial x} - S_0 + S_f = 0 \quad (12)$$

in which S_f is the slope of the energy grade line. Inserting (12) into Manning's equation yields an expression for the stream rating curve,

$$V = \frac{C_m}{n} R^{2/3} \left(S_0 - \frac{\partial y}{\partial x} \right)^{1/2} \quad (13)$$

where R is the hydraulic radius, n is Manning's roughness coefficient, and C_m is a constant that is dependent upon the system of units. To obtain a relationship that is consistent with the downstream-progressing discharge calculation of (11), the spatial derivative in (13) is replaced with a quantity determined at a point. If the energy slope is adequately large, arguments from kinematic wave theory can be used, and (13) can be rewritten in a form of the "Jones formula" as

$$V = \frac{C_m}{n} R^{2/3} \left(S_0 + \frac{1}{c^2 B} \frac{\partial Q}{\partial t} \right)^{1/2} \quad (14)$$

We will assume for simplicity a wide rectangular channel, and with a finite difference approximation of the time derivative in (14) the flow depth is

$$y = \left[\frac{Qn}{C_m B (S_0 + (Q - Q_0)/c^2 B \Delta t)^{1/2}} \right]^{3/5} \quad (15)$$

The depth corresponding to a given discharge varies depending upon the evaluation of the water surface slope and is lower during the rising limb of a hydrograph than during the falling portion of the hydrograph. The accuracy of the depth calculation using (15) depends upon the relative magnitudes of the slope terms. In response to decreasing flow in a river reach having a small bottom slope the denominator of (15) may decrease more quickly than the numerator, causing the calculated stage to increase. This unphysical result signals the need for an alternate equation for modeling the flow depth. If the definition of celerity is approximated as

$$c = \frac{dQ}{dA} \approx \frac{\Delta Q}{B\Delta y}$$

then an alternate equation for flow depth is

$$y = y_0 + \frac{1}{cB} (Q - Q_0) \quad (16)$$

The remaining unknown to be determined is wave celerity. The celerity of a kinematic or diffusion flood wave is related to the flow velocity by a multiplier that depends upon the channel shape and energy slope model used [Henderson, 1963]. The wave celerity of steep-fronted tailwater releases is also dependent upon the flow depth on either side of the wave front. In the extreme case of a rapid flow release to a previously dry channel the celerity of the front must equal the velocity of the flow immediately behind it. The monoclinal rising wave is a translatory wave of stable form. If tailwater releases are presumed to be monoclinal waves during passage through a reach Δx , then an expression for wave celerity can be obtained. For a wide rectangular channel, with the Chezy equation used to describe the energy slope, the expression for wave celerity is

$$c_j = \left[\frac{1 - (y_{j+1}/y_j)^{3/2}}{1 - (y_{j+1}/y_j)} \right] V_j \quad (17)$$

For slowly rising hydrographs, (17) yields the familiar result for celerity of a flood wave: $c = 1.5 V$.

The diffusion wave tailwater model is composed of coupled nonlinear equations that are solved simultaneously. To advance the computation in time, (11) is solved at each grid point by using values of Q and c from the previous time step to evaluate the coefficients. The calculation for Q is explicit, progressing in the downstream direction from a known flow at the upstream boundary and given initial conditions. The values of flow depth and celerity are then updated with (15) through (17). A converged solution is reached when computed flows at successive iterations agree within a set tolerance at each location in the numerical grid. In simulations performed at small Courant numbers a good initial estimate of the solution is available from the previous time step, and convergence is generally rapid.

ANALYSIS OF THE MODEL

The development of a numerical model should include a thorough analysis of the solution technique. Simulations per-

formed with a model assuming different numerical parameter values will generally confirm their pronounced effects upon model stability, diffusion, and dispersion, which must be understood to obtain accurate solutions that can be readily interpreted. In the diffusion wave model, grid parameters Δx and Δt and the weight parameter θ must be specified. The capability of the model is enhanced by using θ to enforce the balance between physical and numerical diffusion and by specifying a numerical grid that adequately resolves the flow waves of interest, conserves mass, and minimizes the imbalance between physical and numerical dispersion.

Modified Equation and Hirt Analyses

The stability, damping, and dispersion characteristics of a difference approximation to a partial differential equation can be investigated with the modified equation analysis of *Warming and Hyett [1974]* and with the Hirt analysis. The two analyses follow the same basic steps with one important difference. Neglecting roundoff error, the modified equation represents the actual partial differential equation solved when a numerical solution is obtained from a difference equation. To obtain the modified equation for the difference scheme of (11), we expand each term in a Taylor series about Q_j^m . Upon simplification, the resulting equation is

$$\frac{\partial Q}{\partial t} + c \frac{\partial Q}{\partial x} + \frac{c\Delta x}{2} \frac{\partial^2 Q}{\partial x^2} + \frac{\Delta t}{2} \frac{\partial^2 Q}{\partial t^2} + \frac{c\Delta t}{(1-\beta)} \frac{\partial^2 Q}{\partial x \partial t} + \frac{c\Delta x^2}{6} \frac{\partial^3 Q}{\partial x^3} + \frac{\Delta x^2}{2\alpha} \frac{\partial^3 Q}{\partial x^2 \partial t} + \frac{\Delta x \Delta t}{2\alpha} \frac{\partial^3 Q}{\partial x \partial t^2} + \frac{\Delta t^2}{6} \frac{\partial^3 Q}{\partial t^3} + \left(\begin{matrix} \text{higher-order} \\ \text{terms} \end{matrix} \right) = 0 \tag{18}$$

The modified equation has an infinite number of terms. Terms appearing in the modified equation but missing from the original differential equation represent a type of truncation error.

Properties of a difference scheme can be found by examining a truncated version of the modified equation. The time derivatives higher than first order and the mixed derivatives are eliminated from (18) to obtain an equation that is amenable to physical interpretation. Even-order spatial derivatives in the recast equation correspond to dissipative effects, and odd-order spatial derivatives reveal dispersive properties of the model. In the Hirt analysis the governing differential equation is used to simplify (18). However, a solution of the original differential equation will not, in general, satisfy the difference equation. Therefore, in the modified equation approach, (18) itself is differentiated and used in the simplifying process. The coefficients are assumed to be constant in both analyses. Differences between the two procedures for the diffusion wave model analysis appear in the coefficients of third- and higher-order spatial derivatives.

Following the modified equation approach, (18) becomes

$$\frac{\partial Q}{\partial t} + c \frac{\partial Q}{\partial x} = D \frac{\partial^2 Q}{\partial x^2} + E \frac{\partial^3 Q}{\partial x^3} + \left(\begin{matrix} \text{higher-order} \\ \text{terms} \end{matrix} \right) \tag{19}$$

$$D = \frac{c\Delta x}{2} \left(\frac{2C_r}{1-\beta} - 1 - C_r \right)$$

$$E = \frac{c\Delta x^2}{6}$$

$$\left[3C_r \left(\frac{2}{1-\beta} - 1 \right) - 1 - 2C_r^2 \left(1 - \frac{3}{1-\beta} + \frac{3}{(1-\beta)^2} \right) \right]$$

Following Hirt's analysis, the analogous expression for E is

$$E_H = \frac{c\Delta x^2}{6} \left[3C_r \left(\frac{1}{1-\beta} \right) - 1 - C_r^2 \left(\frac{3}{1-\beta} - 1 \right) \right] \tag{20}$$

The modified equation can be rewritten in the form

$$\frac{\partial Q}{\partial t} = \sum_{p=0}^{\infty} \mu(2p+1) \frac{\partial^{2p+1} Q}{\partial x^{2p+1}} + \sum_{p=1}^{\infty} \mu(2p) \frac{\partial^{2p} Q}{\partial x^{2p}} \tag{21}$$

The form of the solution of (21) is

$$Q(x, t) \approx e^{(a+ib)t} e^{ikx} \tag{22}$$

$$a = \sum_{p=1}^{\infty} (-1)^p k^{2p} \mu(2p) \quad b = \sum_{p=0}^{\infty} (-1)^p k^{2p+1} \mu(2p+1)$$

where k is the wave number ($2\pi/\text{wavelength}$) of the solution component, and $i = \sqrt{-1}$.

As waves of large wave number cannot be resolved on a numerical grid, waves with small wave numbers are of primary importance. For these waves the exponent a of (22) can be approximated as

$$a \approx -k^2 D \tag{23}$$

where D is the diffusion coefficient defined in (19). A dimensionless numerical diffusion coefficient $D^* = D/(c\Delta x)$ of the diffusion wave model is given in Figure 1 as a function of the Courant number for various values of θ . For Courant numbers less than 0.5, damping is not a strong function of the Courant number. A positive diffusion coefficient in the modified equation, necessary for a stable numerical solution, is obtained if either $0 \leq \theta \leq 0.5$ or $C_r \geq 1.0$ and $\theta < 1.0$. Numerical dissipation increases as θ decreases and as C_r increases. Therefore, stability does not restrict either the minimum value of θ or the maximum value of the Courant number, presenting the possibilities of allowing negative θ and large time steps in the model.

Equation (5), describing wave movement in rivers, has the same form as (21). Analysis of (5) revealed that flow in natural rivers is adequately described by including terms through second order. The Fourier components of the continuum solution of the resulting advective diffusion equation are Q_k exp $[ik(x - ct) - Dk^2t]$. Components of all wave numbers are advected at c , and after an increment of time Δt , all components have undergone a phase angle change Φ_c of

$$\Phi_c = -ck\Delta t = -C_r(k\Delta x) = -C_r \gamma \tag{24}$$

In the model, celerity is a function of wave number (22), and the phase angle change of the numerical solution in time Δt is

$$\Phi_N = b\Delta t = -ck\Delta t + \Delta t \sum_{p=1}^{\infty} (-1)^p k^{2p+1} \mu(2p+1) \tag{25}$$

The ratio of the numerical to continuum phase shifts yields an expression for the relative propagation speed of each Fourier component per time increment

$$\Phi_r = \Phi_N / \Phi_c = 1 - \frac{1}{c} \sum_{p=1}^{\infty} (-1)^p k^{2p} \mu(2p+1) \tag{26}$$

Values of Φ_r greater than 1 indicate that the numerical solution component of wave number k will have a celerity greater than that of the continuum solution, with the converse true for values of Φ_r less than 1. Since small wave numbers are of primary importance in the numerical solution, (26) can be

approximated as

$$\Phi_r = 1 + \frac{k^2 \mu(3)}{c} + O(\gamma^4) \approx 1 + \frac{\gamma^2}{6} \left[3C_r \left(\frac{2}{1-\beta} - 1 \right) - 1 - 2C_r^2 \left(1 - \frac{3}{1-\beta} + \frac{3}{(1-\beta)^2} \right) \right] \quad (27)$$

Equation (27) is plotted as a function of the Courant number for selected values of θ in Figures 2-4 for wavelengths of $24 \Delta x$, $12 \Delta x$, and $6 \Delta x$, respectively. At these wavelengths the phase angle of the numerical solution predominantly lags that of the continuum solution. The discrepancy is largest for the shorter wavelengths, smaller values of θ , and larger values

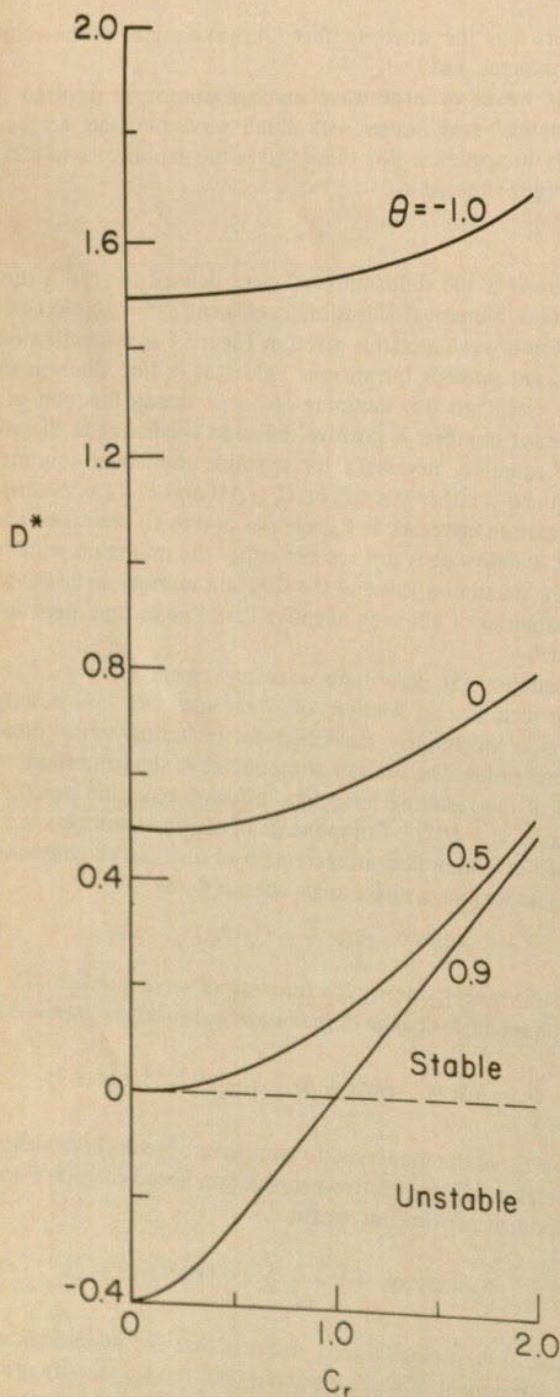


Fig. 1. Dimensionless numerical diffusion coefficient as a function of Courant number for various values of the parameter θ based upon the modified equation analysis.

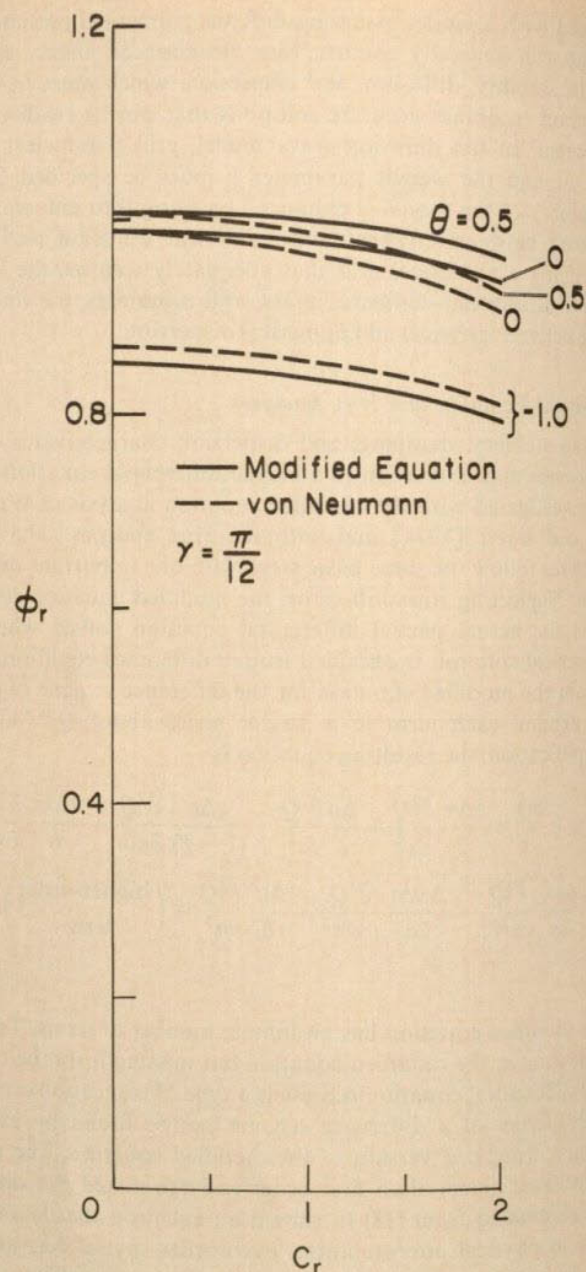


Fig. 2. Ratio of numerical to continuum phase shifts in time Δt for $24\Delta x$ wavelengths as a function of Courant number and various values of θ . One set of curves is based upon the modified equation analysis and one set upon the von Neumann analysis.

of the Courant number. For the shorter wavelengths and Courant numbers greater than 1 the phase angle of the numerical solution varies strongly with the Courant number. The numerical solution is most likely to exhibit leading phase angles for waves of short wavelength with θ approximately 0.5 and Courant number less than 0.5.

An analogous equation for the ratio of the numerical to continuum phase shifts based upon the Hirt analysis can be written by substitution of (20) for $\mu(3)$ of (27), yielding

$$\Phi_r \approx 1 + \frac{\gamma^2}{6} \left[3C_r \left(\frac{1}{1-\beta} \right) - 1 - C_r^2 \left(\frac{3}{1-\beta} - 1 \right) \right] \quad (28)$$

Equation (28) is plotted in Figure 5 as a function of the Courant number for the same wavelengths and θ values used with (27). This series of curves projects quite different phase behavior than the modified equation analysis. At a Courant number of 1 the Hirt analysis projects zero dispersion independent of

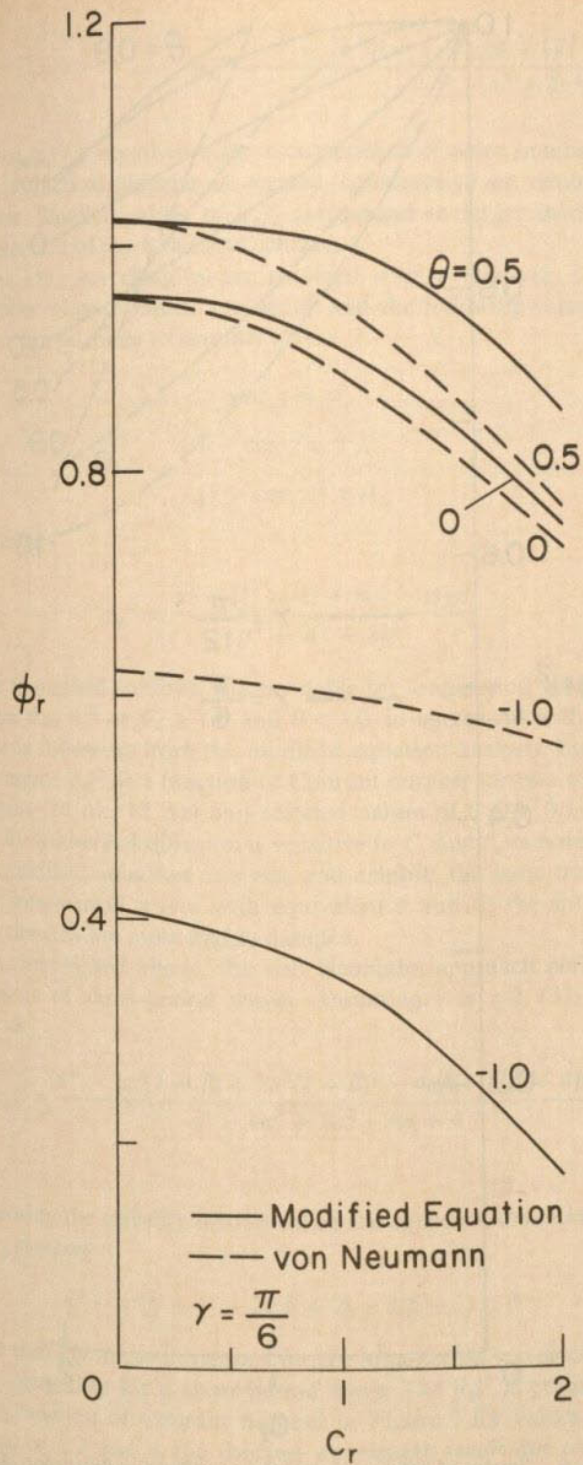


Fig. 3. Ratio of numerical to continuum phase shifts in time Δt for $12\Delta x$ wavelengths as a function of Courant number and various values of θ . One set of curves is based upon the modified equation analysis and one set upon the von Neumann analysis.

wavelength and θ . Lagging phase angles are projected at higher Courant numbers, and all phase angles are leading at lower Courant numbers. Shorter wavelengths and lower values of θ are projected to have larger phase errors.

von Neumann Analysis

As a result of the truncation of terms in (23) the modified equation analysis does not provide information regarding the diffusive nature of the short-wavelength Fourier components of the solution or of the errors that, at times, are responsible for instability of a numerical solution. Similarly, the approxi-

mation in (27) limits the application of the modified-equation-based phase relationship to waves of relatively small wave number. In addition to its usual role of providing numerical stability criteria, the von Neumann analysis can be used to identify the diffusive and dispersive nature of Fourier components of all wave numbers.

The evolution of the numerical solution in a time step Δt is considered in this approach. If the coefficients α and β of (11)

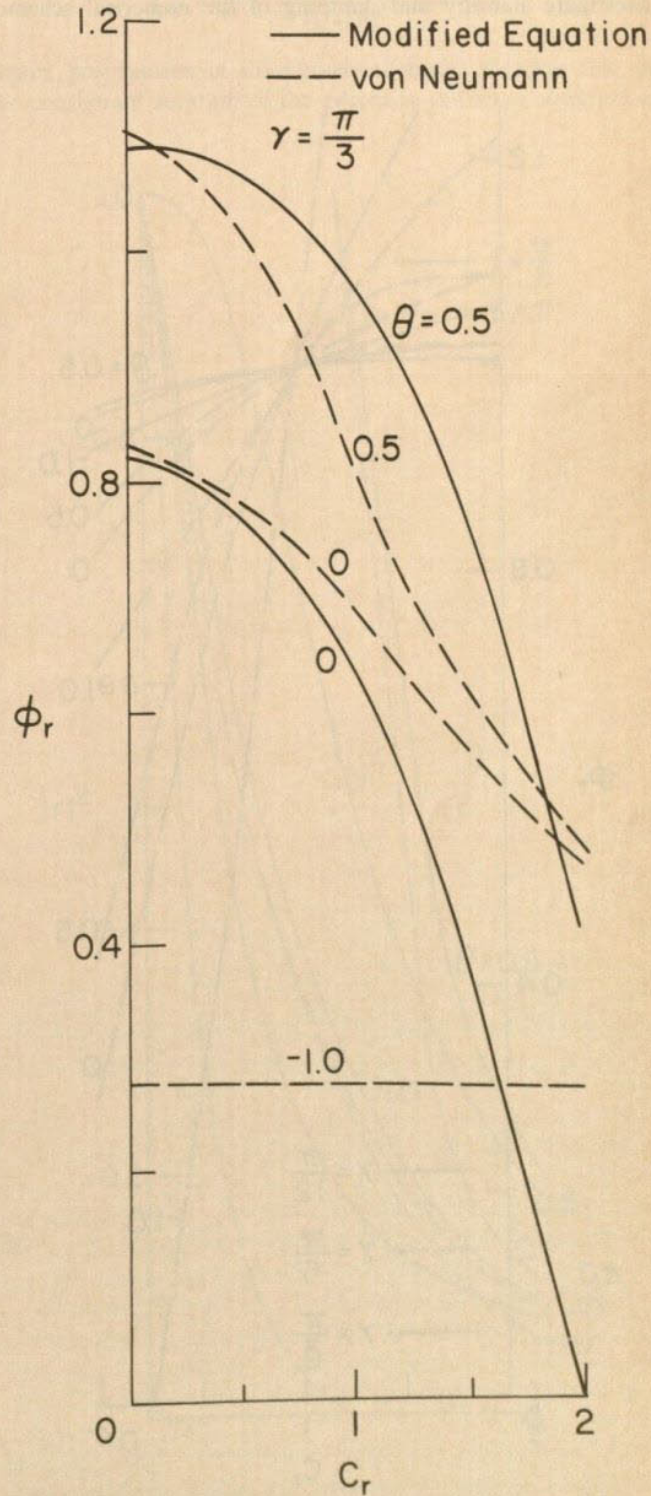


Fig. 4. Ratio of numerical to continuum phase shifts in time Δt for $6\Delta x$ wavelengths as a function of Courant number and various values of θ . One set of curves is based upon the modified equation analysis and one set upon the von Neumann analysis.

are assumed to be constant, the solution can be written as a Fourier series

$$Q_j^m = \sum_k \bar{Q}_k^m e^{ij\gamma} \quad (29)$$

where \bar{Q}_k^m is an amplitude function at time $m\Delta t$ of the Fourier component of wave number k . Each term of the difference equation is replaced by its k th Fourier component, and boundary influences are not considered. The decay or amplification of each component is then evaluated by forming the ratio of the amplitude functions at two successive times to investigate stability and damping of the numerical scheme.

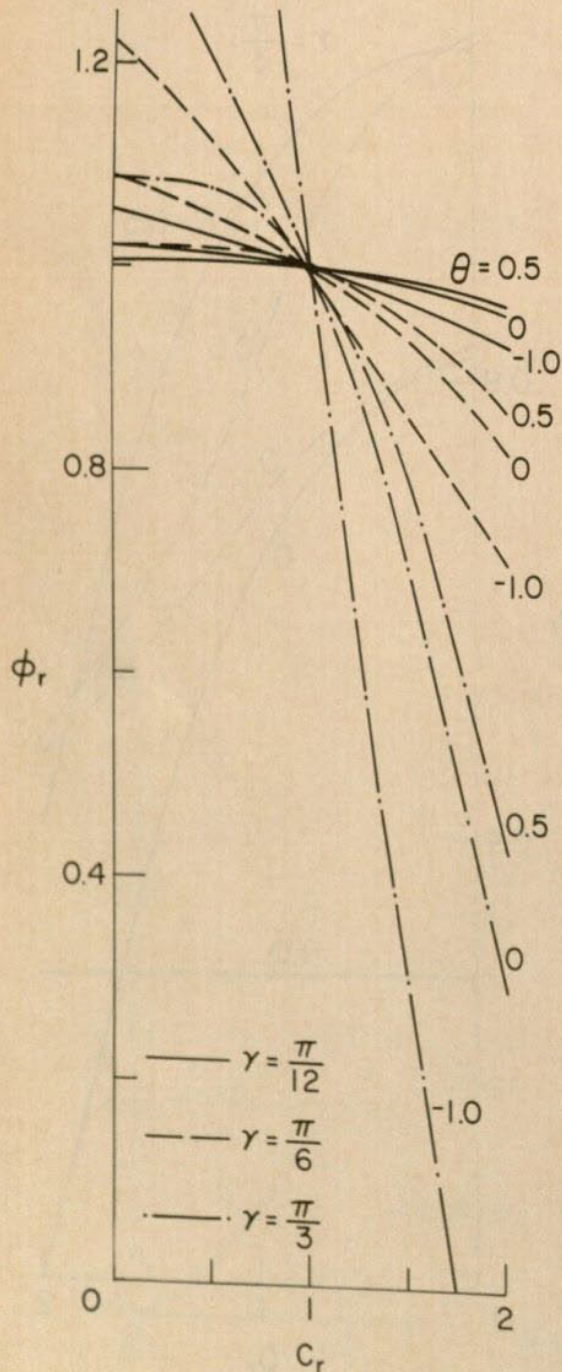


Fig. 5. Ratio of numerical to continuum phase shifts in time Δt for $24\Delta x$, $12\Delta x$, and $6\Delta x$ wavelengths as a function of Courant number and various values of θ based upon the Hirt analysis.

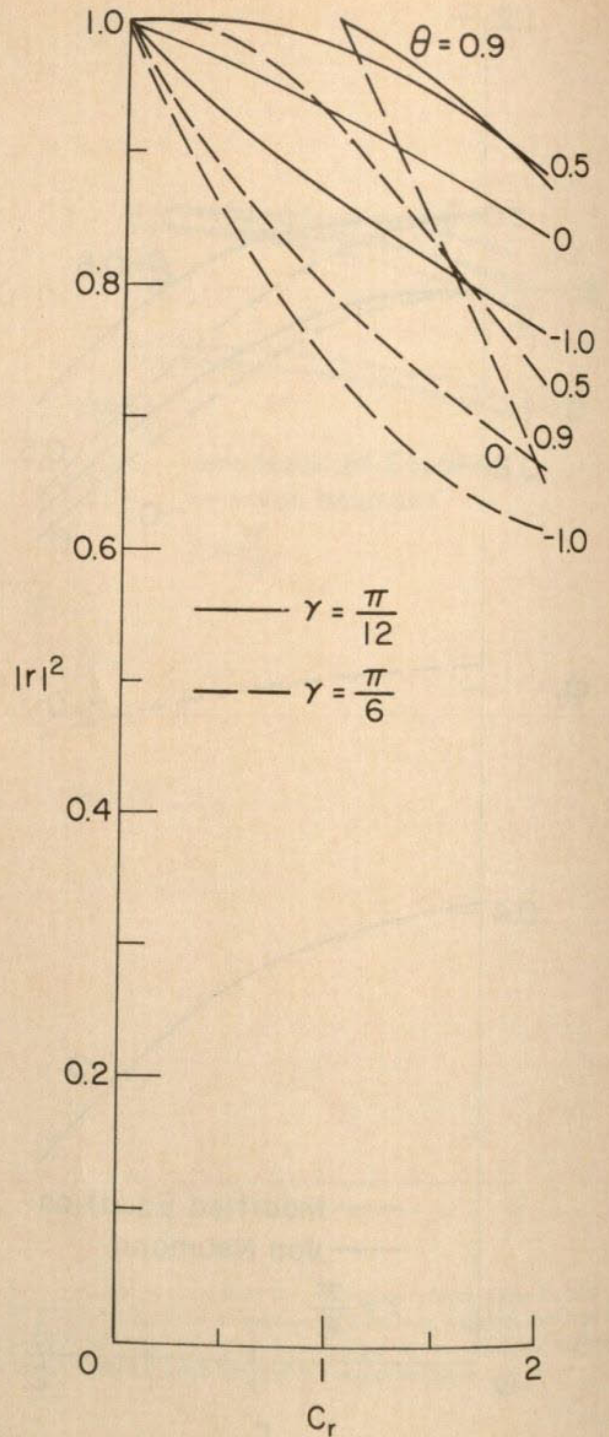


Fig. 6. Square of the modulus of the amplification factor for $24\Delta x$ and $12\Delta x$ wavelengths as a function of Courant number and various values of θ .

Performing these operations upon (11) yields

$$r_k = \frac{\bar{Q}_k^{m+1}}{\bar{Q}_k^m} = \frac{\alpha + \beta(e^{i\gamma} - 1)}{\alpha + (e^{i\gamma} - 1)} \quad (30)$$

in which the complex number r_k is termed the amplification factor. A necessary and sufficient condition for stability of the solution is that the modulus of r_k be less than or equal to 1 for all integer values of k [Richtmyer, 1957]. It follows that the square of the modulus of r_k must also remain less than or equal to 1 for a stable numerical solution, which from (30) is

$$|r_k|^2 = \frac{\alpha^4 + 2\alpha^2(\beta + 1 - \alpha)(\beta + 1)(1 - \cos \gamma) + 2\beta[2\beta(1 - \alpha) + \alpha(\alpha - 2)](1 - \cos \gamma)^2 - 2\alpha^2\beta \sin^2 \gamma}{\alpha^4 + 4\alpha^2(1 - \alpha)(1 - \cos \gamma) + 4(1 - \alpha)^2(1 - \cos \gamma)^2} \quad (31)$$

When $|r_k|^2$ is equal to 1 for a component of wave number k , the numerical scheme is termed conservative or neutrally stable. Smaller values of $|r_k|^2$ correspond to larger inherent dissipation of the numerical scheme.

As long wavelengths are resolved over a relatively large number of grid points, γ is small, and the following substitutions can be made to simplify (31):

$$\begin{aligned} \sin^2 \gamma &\approx \gamma^2 \\ 1 - \cos \gamma &\approx \gamma^2/2 \\ (1 - \cos \gamma)^2 &\approx 0 \end{aligned} \quad (32)$$

yielding

$$|r_k|^2 \approx \frac{\alpha^2 + [(1 - \alpha) + \beta(\beta - \alpha)]\gamma^2}{\alpha^2 + 2(1 - \alpha)\gamma^2} \quad (33)$$

The numerical solution will be stable for long-period waves if either $\theta \leq 0.5$ or $C_r \geq 1.0$ and $\theta < 1.0$, in agreement with the criteria following from the modified equation analysis. Figure 6 presents $|r_k|^2$ as a function of Courant number for two wavelengths ($24 \Delta x$, $12 \Delta x$) and selected values of θ (0.9, 0.5, 0.0, -1.0). Numerical diffusion is sensitive to C_r and θ , as noted in the modified equation analysis, and exhibits the same trends. For long-period waves with equivalent θ and C_r , the shorter wavelengths are more highly damped.

As mentioned above, the von Neumann approach permits analysis of short-period waves. Assuming γ is $\pi/2$, (31) becomes

$$|r_k|^2 = \frac{\alpha^4 - 2\alpha^3(1 + \beta) + 2\alpha^2(1 + \beta)^2 - 4\alpha\beta(1 + \beta) + 4\beta^2}{\alpha^4 - 4\alpha^3 + 8\alpha^2 - 8\alpha + 4} \quad (34)$$

Imposing the stability restriction on the square of the modulus of r_k requires

$$\alpha^3 - \alpha^2(\beta + 3) + 2\alpha(\beta + 2) - 2(\beta + 1) \leq 0 \quad (35)$$

The stability limits developed for the long-period waves satisfy this inequality for a short-period wave. The $|r_k|^2$ is presented as a function of Courant number in Figure 7 for values of γ equal to $\pi/2$ and π , the shortest wavelength resolvable on the numerical grid. Short-period wave damping increases with Courant number and with decreasing wavelength and is a much stronger function of Courant number than that for long-period waves. Wave propagation with a Courant number of 1.0 and θ of 0.9 is undamped for both short- and long-period waves.

The dispersive properties of the numerical scheme can also be investigated by using the von Neumann analysis. For small angles the measure of an angle in radians is approximately equal to the sine of the angle. The phase angle of the numerical solution at time Δt is then

$$\Phi_N = \frac{\text{Imag}(r_k)}{|r_k|} \quad (36)$$

For the diffusion wave model the ratio of the numerical to

continuum phase angle is formed with (24) and (36), yielding

$$\Phi_r = \frac{\sin \gamma}{\gamma} \left[\frac{1}{1 + 2A + A^2 + C_r^2 \sin^2 \gamma} \right]^{1/2} \quad (37)$$

where

$$A = \frac{C_r(\beta^2 + 2\beta C_r - 1)(1 - \cos \gamma)}{(1 - \beta)^2}$$

Again, propagation in the numerical model matches that in the continuum solution of the advective diffusion equation if

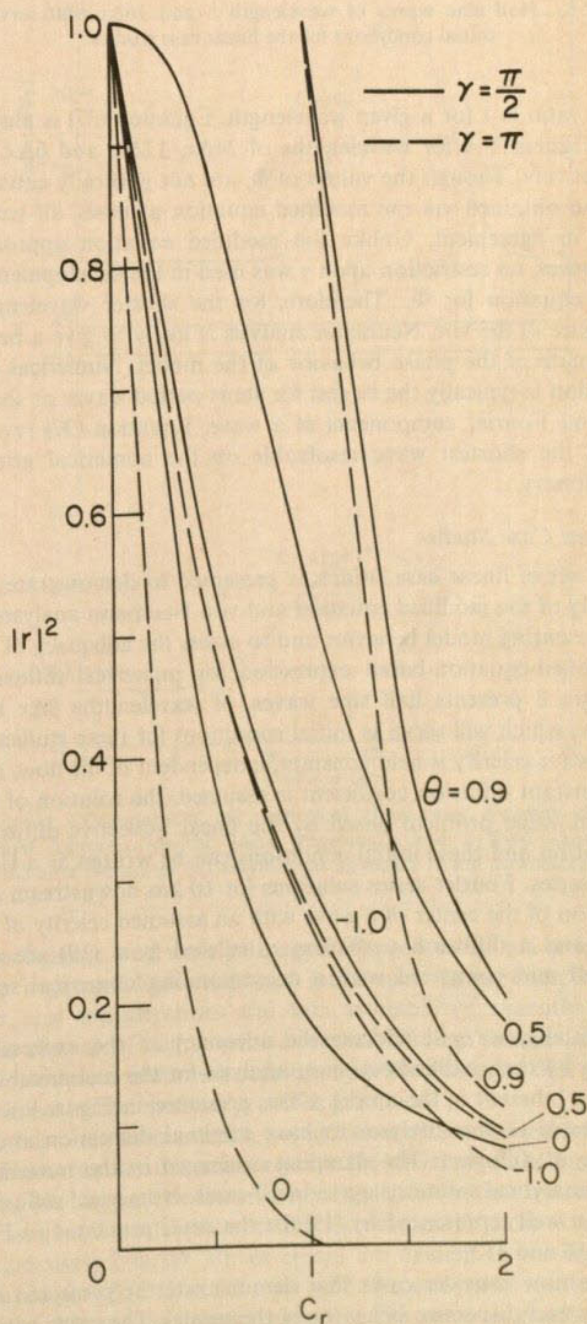


Fig. 7. Square of the modulus of the amplification factor for $4\Delta x$ and $2\Delta x$ wavelengths as a function of Courant number and various values of θ .

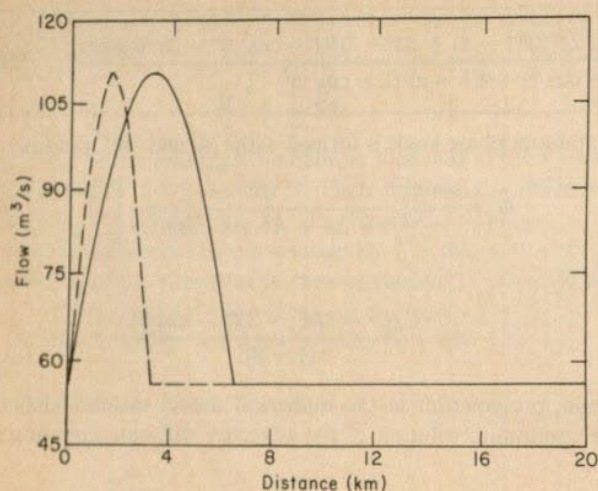


Fig. 8. Half sine waves of wavelength 8 and $16\Delta x$ that serve as initial conditions for the linear case studies.

this ratio is 1 for a given wavelength. Equation (37) is plotted in Figures 2-4 for wavelengths of $24\Delta x$, $12\Delta x$, and $6\Delta x$, respectively. Though the values of Φ_r are not generally equal to those obtained via the modified equation analysis, all trends are in agreement. Unlike the modified equation approach, however, no restriction upon γ was used in the development of the equation for Φ_r . Therefore, for the shorter wavelengths (Figure 4) the von Neumann analysis is likely to give a better estimate of the phase behavior of the model. Numerical dispersion is typically the largest for short-period waves or short-period Fourier components of a wave. Equation (37) reveals that the shortest wave resolvable on the numerical grid is stationary.

Linear Case Studies

A set of linear case studies is presented to demonstrate the utility of the modified equation and von Neumann analyses in representing model behavior and to assess the adequacy of the modified-equation-based expression for numerical diffusion. Figure 8 presents half sine waves, of wavelengths $8\Delta x$ and $16\Delta x$, which will serve as initial conditions for these studies. If the wave celerity is held constant, independent of the flow, and a constant diffusion coefficient is assumed, the solution of the initial value problem posed by the linear advective diffusion equation and these initial conditions can be written as a Fourier series. Fourier series solutions for 10 km downstream advection of the center of a wave with an assumed celerity of 0.9 m/s and a diffusion coefficient calculated from (19) are obtained and compared with a corresponding numerical solution.

Initially, we will address the adequacy of the expression given by the modified equation analysis for the numerical diffusion inherent in the model. Cases presented in Figure 9 were projected in the analyses to have minimal dispersion and a range of diffusion. The damping evidenced in the numerical and analytical solutions agree in all cases. Numerical diffusion is also well represented by (19) for the cases presented in Figures 10 and 11.

We now consider cases that demonstrate the projected diffusive and dispersive behavior of the model. The cases with θ equal to 0.9 and C_r of 1.0 (Figure 9) exhibited essentially pure advection. No damping or phase error of any Fourier component of the solution was projected for this case by the von Neumann analysis. A small amount of dispersion, evidenced

by a slight lag in the numerical solution, was present in the cases with θ of 0.0 and C_r of 0.1 (Figure 9). This slight lagging phase error was projected by both the von Neumann and modified equation analyses (Figures 2 and 3). The Hirt analysis incorrectly projected a leading phase error for these same cases (Figure 5). Figure 10 contains numerical and analytical solution comparisons for cases with a constant Courant number and selected values of θ . The leading phase error of the longer-wavelength components and the more extreme leading phase error of the short-wavelength components are evident for the case in which θ is 0.5, as projected in Figures 3 and 4. Minimal damping of the short-wavelength components (Figure 7) is a necessary condition for development of leading short-period waves. A small amount of phase lag occurred as projected for the case with θ equal to 0.0. Larger damping and

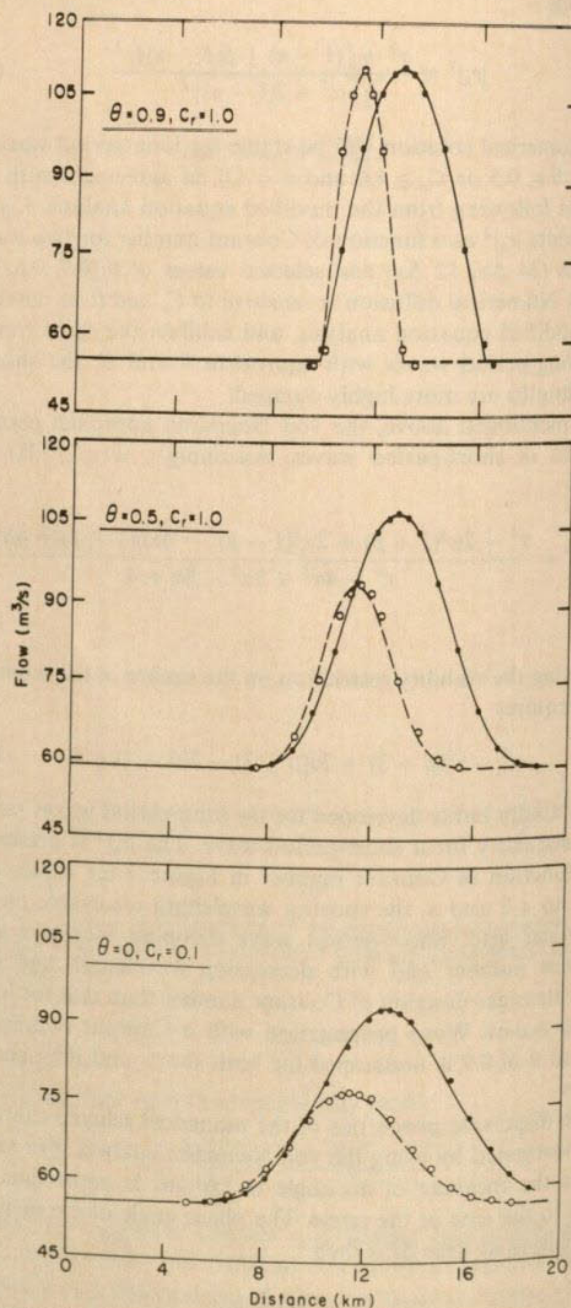


Fig. 9. Comparison of numerical (lines) and Fourier series (points) solutions for the 8 and $16\Delta x$ wavelengths after the center of the wave has advected 10 km downstream. Cases shown were projected to have minimal dispersion and a range of diffusion by the modified equation and von Neumann analyses.

greater phase lag accompanied a reduction of θ to -1.0 . The Hirt analysis projections of leading phase errors for all θ values when the Courant number is small and for the more extreme leading phase errors with negative θ are, again, incorrect. For the cases presented in Figure 11, θ is held constant as Courant number is varied. As projected by the modified equation and von Neumann analyses, leading phase errors of the short-wavelength components occurred for Courant number 0.1; lagging phase errors occurred for Courant number 4.0; and a minimal phase error was observed for Courant number 1.0.

Numerical Mesh Selection

Assessment of the adequacy of a numerical mesh is an important problem-dependent part of model development. As revealed by further studies of the laboratory, rapidly varying flow tests reported by Ferrick [1980], diffusion wave model

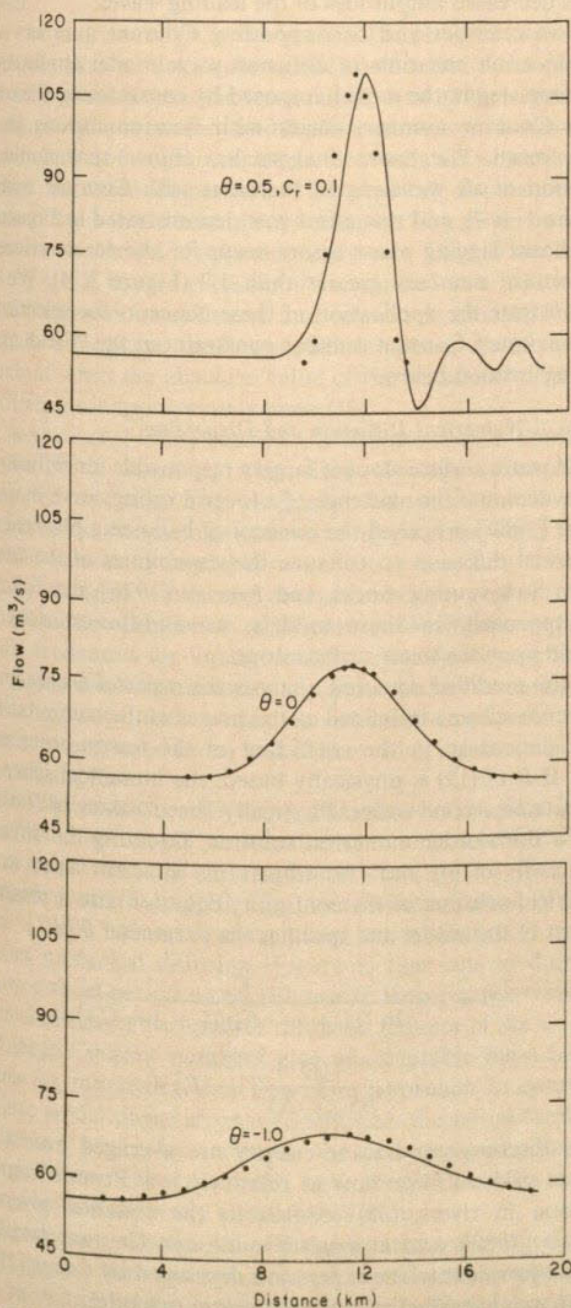


Fig. 10. Comparison of numerical (line) and Fourier series (points) solutions for the $8\Delta x$ initial wavelength and a fixed value of $C_r = 0.1$ after the center of the wave has advected 10 km downstream.

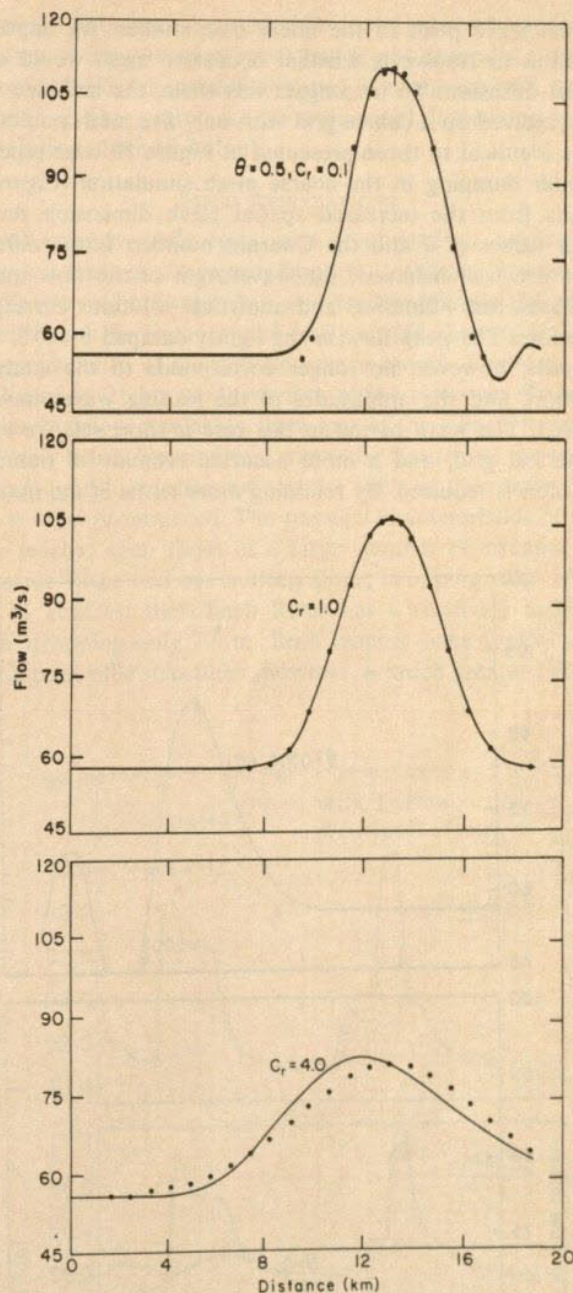


Fig. 11. Comparison of numerical (line) and Fourier series (points) solutions for the $16\Delta x$ wavelength and a fixed value of $\theta = 0.5$ after the center of the wave has advected 10 km downstream.

mass balance, and wave propagation speed errors are reduced with improved numerical grid refinement. In practice, however, cost considerations and data availability frequently preclude the use of highly refined meshes. Though numerical experimentation with mesh refinement is the final test of a grid, the linear model analysis provides guidance.

A basic requirement of a numerical mesh for tailwater flow studies is that it adequately resolve the wavelengths of interest in the prototype. The linear analysis has shown that numerical diffusion and model phase errors increase as the mesh is made progressively coarser. Phase errors are evident in the lightly damped $\theta = 0.5$, $C_r = 0.1$ case with 9-mesh-point resolution (Figure 10) and to a lesser extent in the same case with 17-point resolution (Figure 11). These same mesh resolutions exhibit little phase error in cases with increased diffusion (Figures 10-11).

The 9- and 17-mesh point wave resolutions retained the

correct wave peak in the linear case studies. An important question to resolve is whether a coarser mesh would affect model diffusion. To investigate this effect, the half sine wave was resolved on a coarse grid with only five mesh points, and cases identical to those presented in Figure 10 were repeated. Greater damping in the coarse mesh simulation (Figure 12) results from the increased spatial mesh dimension Δx , for given values of θ and the Courant number. Large diffusion cases are well behaved; the wavelength of the flow quickly increases, and numerical and analytical solutions correspond as before. The peak flow in the lightly damped $\theta = 0.5$, $C_r = 0.1$ case, however, no longer corresponds to the analytical solution, and the amplitudes of the leading waves have increased. The wave period in this case is short relative to the numerical grid, and a more accurate estimate of numerical diffusion is required. By retaining more terms of the modified

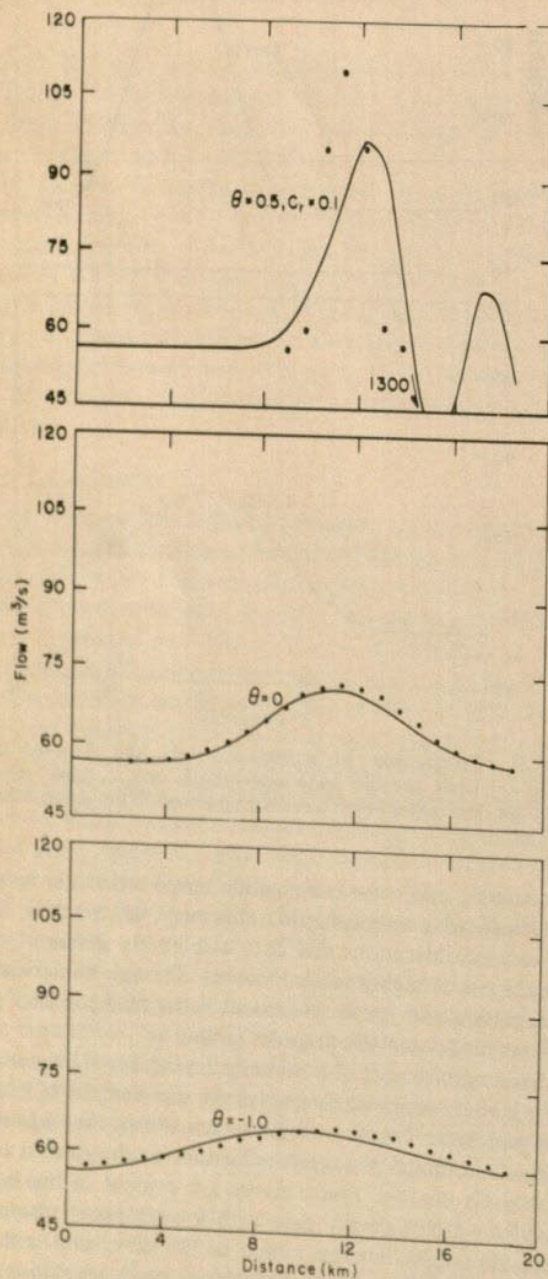


Fig. 12. Comparison of numerical (line) and Fourier series (points) solutions for the coarse grid $4\Delta x$ initial wavelength and a fixed value of $C_r = 0.1$ after the center of the wave has advected 10 km downstream.

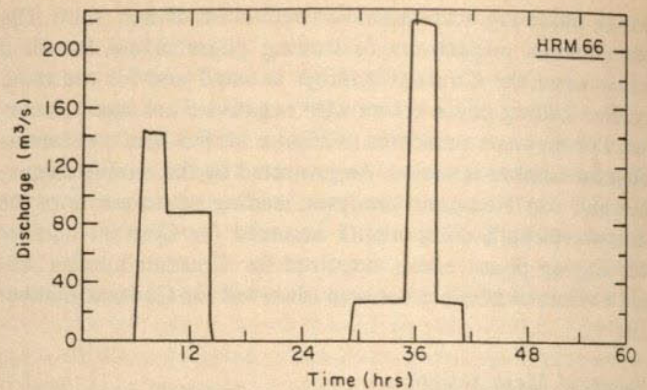


Fig. 13. Apalachia Dam flow releases, March 22-23, 1979.

equation, a higher-order estimate of diffusion could be made. However, a refined mesh corrects the wave peak error and yields decreased amplitudes of the leading waves.

Wave celerities and corresponding Courant numbers vary with location and time in diffusion wave model applications. The time step in the model, imposed by constraining the maximum Courant number, varies with flow conditions in the study reach. The linear analysis has shown that numerical diffusion of all wavelengths increases with Courant number (Figure 1, 6, 7), and this effect was demonstrated in Figure 11. Significant lagging phase errors occur for shorter wavelengths at Courant numbers greater than 1.0 (Figure 3, 4). We will demonstrate the application of these concepts for selection of the maximum Courant number constraint in the "Field Applications" section below.

Physical/Numerical Diffusion and Dispersion

The water surface slope is largely responsible for diffusion of flow waves and the existence of a looped rating curve in rivers. Cunge [1969] proposed the concept of balancing physical and numerical diffusion to enhance the capabilities of the Muskingum flow routing model, and Koussis [1976] also followed this approach. In these models, wave diffusion does not depend upon the water surface slope.

In the modified equation analysis the order of accuracy of a difference scheme is defined as the power of the computational mesh dimension in the coefficient of the lowest-order error term. If D of (19) is physically based, the numerical scheme is accurate to second order. Physically based values of D and E yield a third-order numerical solution. Equating the diffusion coefficients of (4) and (19) transforms an error term in the numerical solution of the continuity equation into a meaningful part of the model and specifies the parameter θ as

$$\theta = 1 + \frac{C_r}{\ln [(1 + \lambda - C_r)/(1 + \lambda + C_r)]} \quad (38)$$

$$\lambda = \frac{\langle \bar{Q} \rangle}{BS_0 \langle \bar{c} \rangle \Delta x} (1 - F^2/4)$$

where discharge and wave celerity are averaged over a numerical grid cell. For flow at relatively low Froude numbers common in rivers, (38) reduces to the equation given by Koussis [1980], and at small Froude and Courant numbers, (38) is equivalent to the expression developed by Cunge [1969] for the weighting factor in the Muskingum model

$$\theta = \frac{1}{2} \left(1 - \frac{\langle \bar{Q} \rangle}{BS_0 \langle \bar{c} \rangle \Delta x} \right) \quad (39)$$

The parameter θ provides variable diffusion in the model when it is continually updated at each point in the numerical mesh. We have demonstrated that model diffusion also depends upon the Courant number. Larger Courant numbers generate increased damping, but (38) compensates by increasing θ to maintain the balance between physical and numerical diffusion. If the Courant number is increased further, θ calculated from (38) may exceed the upper bound for model stability, and small values of diffusion cannot be attained in the model. If the diffusion balance is not enforced, the accuracy of the model is degraded.

Strupczewski and Kundzewicz [1980] and Dooge et al. [1982] found, in analyses of the Muskingum model, that negative values of the weighting parameter are due to short model reach lengths. The same conclusion can be drawn from the value of θ expressed in (38) and (39). If negative values occur, θ can no longer be considered a weighting parameter. Instead, it is a parameter used to control the diffusion of the numerical model.

In the interest of further enhancing the physical basis of the diffusion wave model, equating the coefficients of the physical and numerical dispersion terms of (4) and (19), respectively, would provide improved model phase accuracy. However, the model does not contain another free variable with which to enforce balanced dispersion. The physical dispersion coefficient of (4) is small and always positive. The dispersion coefficient in the model is approximately zero for θ of about 0.25 and $C_r \leq 0.5$. Larger values of θ correspond to a positive numerical dispersion coefficient, and conversely, smaller θ values indicate a negative coefficient. Model phase errors become apparent when the absolute value of the numerical dispersion coefficient is inappropriately large (19).

Chang et al. [1983] studied the diffusion wave model applied to flood waves in rivers. They reported an unphysical computed discharge that decreased below an initial steady state prior to the passage of a wave for positive θ and recommended increasing model time step as a corrective measure. Lightly damped waves are characterized by positive θ and small Courant number or Δt (Figure 1). We have experienced model tendencies for lightly damped, rapidly varying flow of decreasing discharge immediately prior to an increasing flow with the subsequent generation of small-amplitude, short-period leading wave trains and of increasing discharge prior to a decreasing flow.

The development of leading phase errors of short-period wave components was projected in the model analysis (Figure 4) and demonstrated in the linear case studies for lightly damped waves (Figure 10, 11). The recommendation of Chang et al. [1983] reduces leading phase error (Figure 4) and increases numerical diffusion (Figure 1) that acts to damp remaining short-period waves (Figure 7). However, excessive numerical diffusion disrupts the diffusion balance of the solution, and large Courant numbers give unacceptable mass balance errors for rapidly varying flow. Our approach to control of leading model phase error is to suppress the initial formation of leading waves by retaining the previous computed discharge. Numerical experiments have verified that this mechanism does not adversely affect the solution.

An adequate description of sharp-fronted waves of relatively short period that are encountered in tailwaters may dictate fine resolution of the computational mesh. Negative values of θ , which may then be required for balanced diffusion, will introduce lagging phase error in the simulation that will be noticeable for the shorter wavelengths. Minimization of the

dispersion imbalance is possible for many cases with judicious selection of the numerical mesh and is not generally a serious limitation. Still, the insights obtained from the analysis remain valuable as phase error can be anticipated, improving the interpretation of model output.

FIELD APPLICATIONS

Two extensive field tests were conducted to confirm the analytical findings concerning important physical processes in rapidly varying tailwater flow and to demonstrate the practical utility of the linear model analysis and thereby establish the applicability of the diffusion wave model. The tests were conducted in 21-km study reaches of the Hiwassee River immediately below Apalachia Dam and of the Clinch River immediately below Norris Dam, where the features of the tailwater hydrograph are sharpest and the effect of flow wave diffusion is most pronounced. The physical characteristics of these river reaches span those of a large number of streams. The Hiwassee River bed has a steep slope, dropping over 107 m, and by contrast the Clinch River has a relatively mild bed slope, dropping only 7.6 m. Both reaches have typical alternating pool-riffle structures; however, a much greater percent-

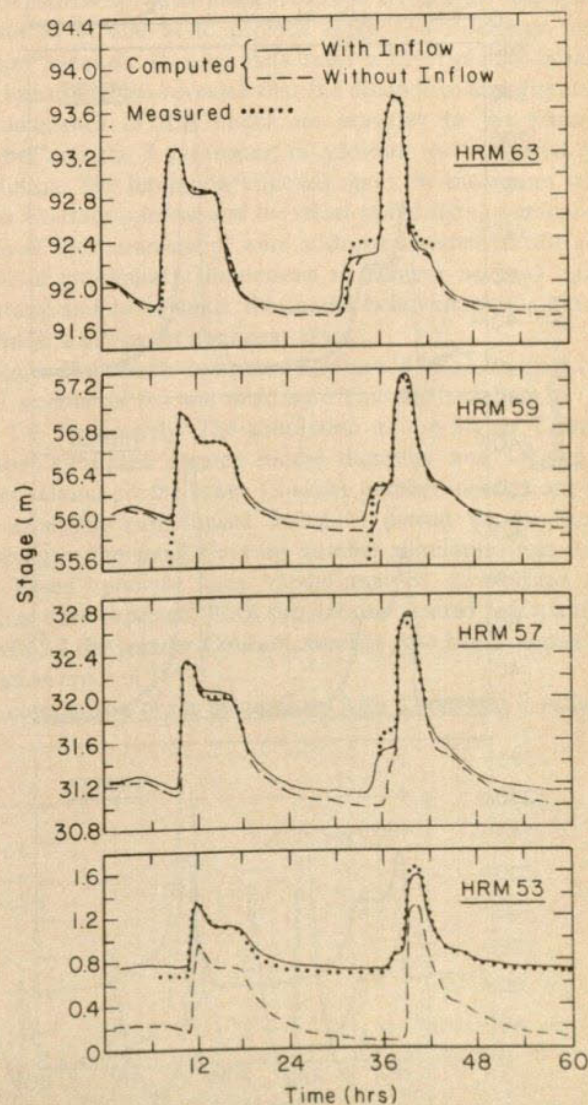


Fig. 14. Measured and computed stage at several locations on the Apalachia tailwater. A maximum Courant number of 1.0, spatial grid resolution of 1600 m, and variable θ limited to positive values were conditions of the numerical simulation.

age of the Norris tailwater is pooled at low flow. The Hiwassee River bed is extremely rough, with large boulders and trees in the channel, creating roughness elements that are typically on the order of the flow depth. In general, roughness elements in the Clinch River reach are much smaller than those of the Hiwassee River reach. Even during lengthy zero-flow release periods from Norris Dam, the roughness elements in the pools remain submerged.

Apalachia Dam Tailwater

Apalachia Dam is situated at Hiwassee River mile (HRM) 66, near the southern end of the Tennessee/North Carolina

border. At the dam the river has a drainage area of 2636 km². The bulk of the flow in this reach is normally diverted from the dam through a conduit to the Apalachia powerhouse, located near the end of the reach. Therefore, flow occurs only during floods and as a result of local inflows from a drainage area totaling 306 km².

A field investigation of flow in the Apalachia Dam tailwater was conducted by the Tennessee Valley Authority (TVA) on March 22–23, 1979. The hydrograph during this study was produced with sluice gates at the dam and is given in Figure 13. River stage was recorded at HRM 62.8, 59.0, 56.9, and 53.0 during the test. The channel shape was approximated in the model as rectangular throughout the tailwater, and local inflow was initially neglected. Channel width and slope were obtained from USGS quadrangles. The tailwater channel width varied between 46 and 134 m, averaging 85 m, and the channel bed slope varied between 0.0027 and 0.0084. Manning's roughness coefficients, estimated on the basis of field observations and adjusted during model calibration, ranged between 0.04 and 0.07, averaging 0.066.

In addition to physical parameters characterizing the reach, model application requires the selection of a numerical grid. The linear analysis and past experience provided guidance in selecting a spatial grid size of 1600 m and a maximum Courant number of 1.0 for application of the model to the Apalachia tailwater. Lagging phase errors associated with negative values of θ were not encountered with these mesh parameters, but relatively light wave damping necessitated the suppression of leading phase errors.

An initial comparison of measured and computed stage is presented in Figure 14. The propagation of the 28-m³/s release in the model lags the data by a time that increases with distance downstream. The timing and magnitude of the other releases are accurately represented in the model. Due to the absence of the powerhouse discharge, the measured and computed stages are not in agreement at HRM 53. Sensitivity studies were conducted in which estimated input parameters, width, and roughness were varied in an effort to improve the agreement between the modeled and measured propagation of the 28-m³/s wave. Increased channel roughness caused a reduction in wave speed, an increase in steady-state stage for a given flow, and an extended duration of the increased stage. Increased channel width caused a decrease in the magnitude of stage changes, a slowing of wave movement, and a decreased period of increased flow. The overall agreement of model and prototype, however, was not improved.

A physically justifiable development that greatly improved the propagation speed of the 28-m³/s wave without significantly affecting the larger waves (Figure 15) was the inclusion of local inflows. Local inflows, measured at 0.35 m³/s km for the 5.6-km reach nearest the dam, were assumed to be representative for the tailwater, and the known discharge at the powerhouse was included as a local inflow. Figure 14 presents a revised comparison between the model and prototype stages. Sensitivity studies indicated that remaining discrepancies in the arrival times of the 28-m³/s wave can be attributed to the lack of detailed inflow data.

At HRM 63 the only discrepancy between computed and observed stages concerns the magnitude of the stage increase during passage of the 28-m³/s wave. The effective channel width at low flow is less than at higher flow, but due to the rectangular channel assumption, measured stage at low flow is higher than the computed stage. At HRM 59 the model accurately describes the prototype stages, except at times when

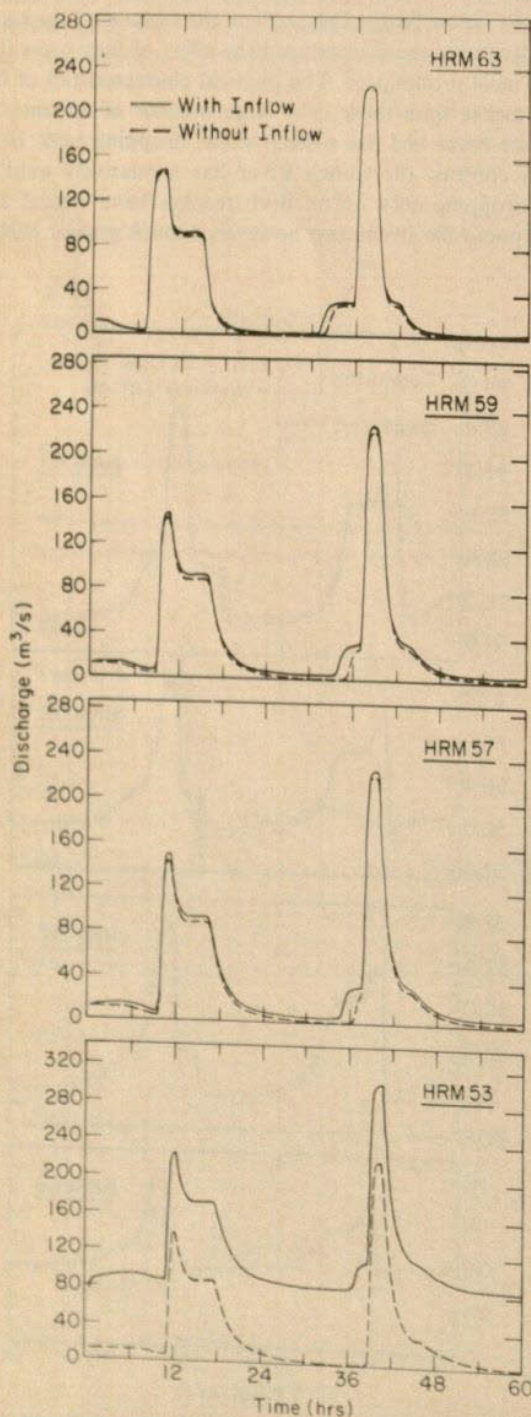


Fig. 15. Computed discharge at several locations on the Apalachia tailwater. A maximum Courant number of 1.0, spatial grid resolution of 1600 m, and variable θ limited to positive values were conditions of the numerical simulation.

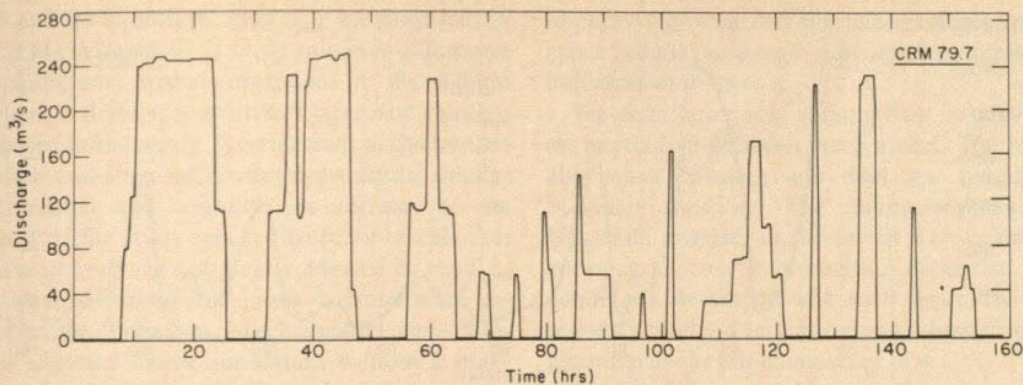


Fig. 16. Norris Dam flow releases, July 1-7, 1980.

only local inflows are present. The river is pooled at low flow at HRM 57, and as a result the computed river stage at this location falls below the measured stage at low flow. At HRM 53, model and prototype stage data agree closely for all the releases. The model accurately conserved mass and reproduced the timing, amplitude, and shape of flow waves throughout the study reach, reflecting favorably upon the numerical mesh parameters used. The physical justification for omission of backwater effects in the model cannot yet be judged. It is possible that the pooled reaches in the Apalachia tailwater were short enough to have a negligible effect upon the flow or that the addition of local inflow compensated for the effect.

Norris Dam Tailwater

Norris Dam is situated at Clinch River mile (CRM) 79.7, near Oak Ridge, Tennessee. The drainage area of the river at the dam is 7542 km². An individual pool located near the center of the study reach is over 4.0 km in length and has a bed slope of only 0.00012. As the diffusion of a flow wave in a wide rectangular channel is inversely proportional to the bed slope (5), we expected much greater diffusion of the flow waves in the Norris tailwater relative to that in the Apalachia tailwater.

A 160-hour controlled release test (Figure 16) was performed in the Norris Dam tailwater by the TVA on July 1-7, 1980, during which the variation of river stage was continuously recorded at CRM 78.85, 76.1, 73.6, 71.4, and 67.3. The long pool in the study reach was isolated by the placement of the recording gages at CRM 76.1 and 73.6. The channel shape was assumed in the model to be rectangular throughout the study reach. Prior to the test, the TVA surveyed the tailwater

for channel width and bed slope. Measured widths ranged between 79 and 165 m, averaging 116 m, and bed slopes varied between 0.00012 and 0.00130. Local inflows were small during the test, averaging about 0.035 m³/s km, with point inflows of 0.54 m³/s from Coal Creek, the largest tributary, and 1.13 m³/s leakage past Norris Dam. Calibrated roughness coefficients used in the model simulations ranged between 0.015 and 0.035, averaging 0.026.

The Norris tailwater model required a relatively fine spatial resolution of 800 m to provide stage and discharge information adequate to accurately resolve short-period releases. The linear analysis revealed that the dissipative and dispersive characteristics of the model are sensitive to the Courant number and the θ parameter, in addition to the spatial grid resolution. The limitation imposed upon the maximum value of the Courant number and the effect of specifying a minimum value of the parameter θ were addressed systematically in a series of preliminary simulations to achieve optimal model accuracy and to evaluate the model behavior predictions of the linear analysis for nonlinear cases.

Figure 17 presents computed flow at CRM 67.2 with a constant θ value of 0.5 and maximum Courant numbers of 0.25 and 1.0, respectively. The simulation at the higher Courant number exhibited greater model damping and lagging of waves relative to the lower Courant number simulation; this was especially pronounced for short period waves. Model damping in the small Courant number simulation was minimal. Based upon the linear model analysis, all of these tendencies were expected. Both simulations created mass, and at CRM 67.2 the smaller Courant number case had a mass conservation error of 28%.

A comparison of the simulations with a constant θ value of

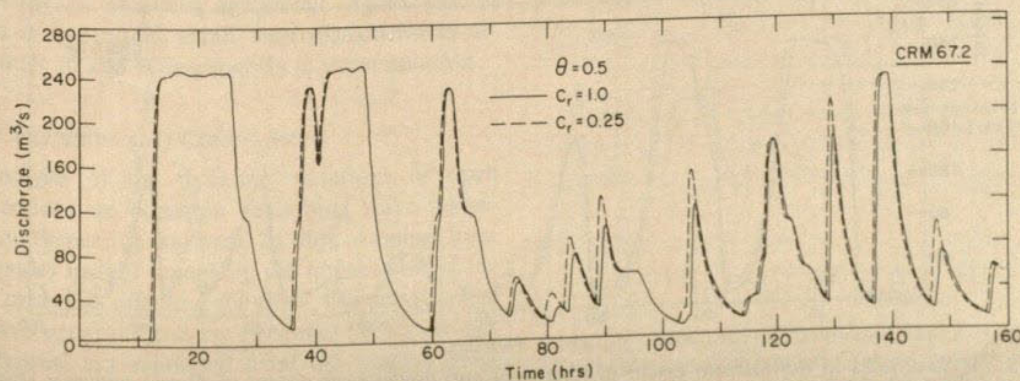


Fig. 17. Hydrographs at downstream extent of Norris tailwater study reach computed with constant $\theta = 0.5$, spatial grid resolution of 800 m, and maximum Courant numbers of 0.25 and 1.0.

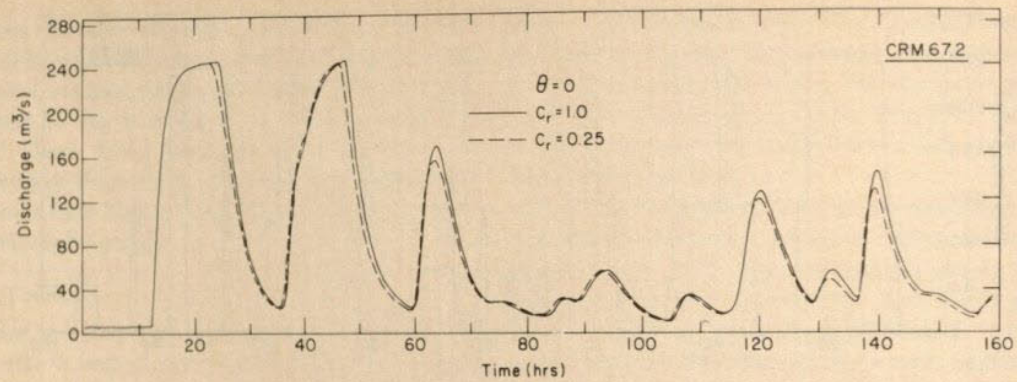


Fig. 18. Hydrographs at downstream extent of Norris tailwater study reach computed with constant $\theta = 0.0$, spatial grid resolution of 800 m, and maximum Courant numbers of 0.25 and 1.0.

0.0, given in Figure 18, shows that wave propagation was slightly faster and wave attenuation was greater for the simulation with a maximum Courant number of 0.25 than for the Courant number 1.0 simulation. The apparent contradiction with the linear theory concerning wave attenuation is actually an effect of improved mass conservation, which results from a quicker arrival of the tail of the wave. The bulk of the difference between the two simulations occurred in the long, nearly flat, pooled reach. Again, both simulations created mass, but the error was only 4% for the smaller Courant number case. Measured and computed stages with a constant θ value of 0.0 and a maximum Courant number of 0.25 agree reasonably well at all gages, although modeled damping is generally less than that in the prototype. Insufficient numerical diffusion is an indication that negative θ values are needed to maintain the physical-numerical diffusion balance, and satisfactory model accuracy suggests that a variable weighting factor is not essential for modeling flat, ponded river reaches.

Further reduction of the Courant number did not affect the computed hydrograph at the downstream end of the study

reach for any of the constant θ runs. Larger Courant number (≥ 2.0) simulations were attempted, but the model did not converge to a solution at the initial abrupt flow increase of the inflow hydrograph. This convergence problem was not resolved because of generally poor model accuracy at large Courant numbers for rapidly varying flow.

Comparing the simulations of like Courant number in Figures 17 and 18 reveals model tendencies caused by varying the θ parameter that were predicted in the linear analysis. The effect upon model damping of varying θ is greater than the effect of varying the Courant number. For the cases in which θ is set at 0.0 the slopes of wave fronts are less steep, corresponding to increased diffusion relative to the cases where θ is 0.5. Also, the arrivals of the short wavelengths at CRM 67.2 are lagged in the θ equal 0.0 cases, relative to the θ equal 0.5 cases.

The linear analysis indicated that negative values of θ , required to maintain the diffusion balance when fine numerical grids are used, introduce a lagging phase error in the modeled results. Computed hydrographs for simulations having a θ_{min}

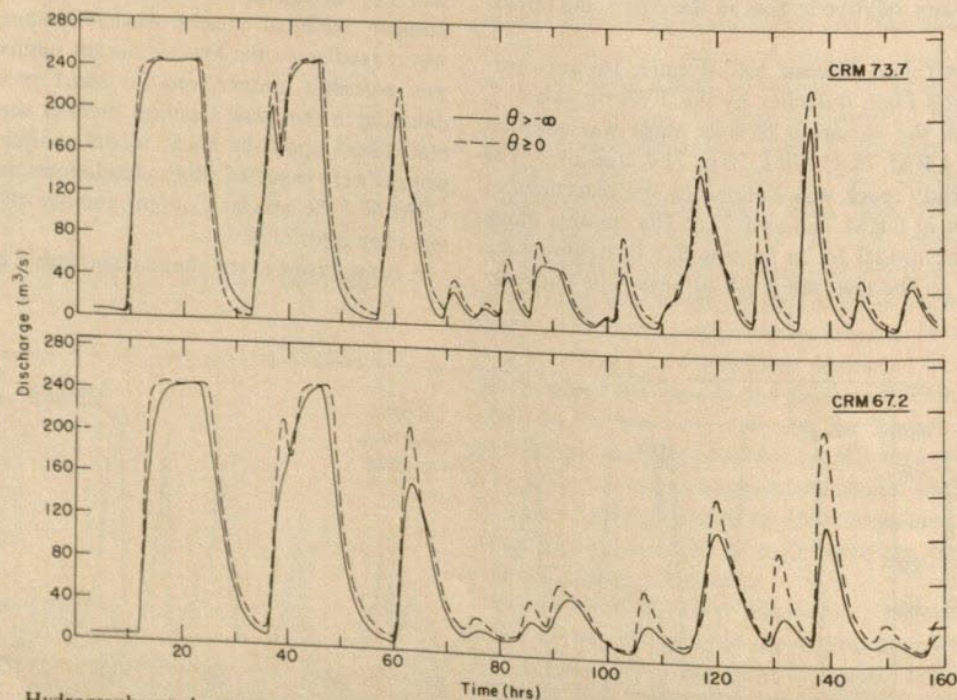


Fig. 19. Hydrographs at downstream extent of long pool and downstream extent of Norris tailwater study reach computed with maximum Courant number of 0.25, spatial grid resolution of 800 m, and variable θ either limited to positive values or allowing negative values.

limitation of 0.0 and no limitation upon θ_{\min} are presented in Figure 19 for CRM 73.7 and 67.2. Only minimal differences between the simulations existed upstream of the 4.0-km pooled reach where bed slope is relatively large and the θ_{\min} limitation is imposed infrequently. Downstream of the pool at CRM 73.7, the flow and stage differences between the simulations were pronounced and continued to increase to the downstream extent of the study reach. Figure 19 reveals that the timing of wave arrival was not greatly affected by the θ_{\min} limitation, but wave damping and mass balance were extremely sensitive to the limitation. Much greater wave diffusion occurred as expected in the simulation without a minimum θ limitation. Limiting θ to positive values did not produce attenuation of the modeled stage peaks that was adequate to reproduce the prototype stage measurements. Limiting θ to positive values resulted in an increase in mass of 14% at the downstream end of the study reach. Relaxing the θ limitation to be greater than -1.0 reduced the increase of mass to 8%, and removing the limitation altogether yielded a 4% decrease of mass at the downstream end of the reach.

The preliminary Norris tailwater simulations support the validity of model behavior predictions of the linear analysis for nonlinear cases. Optimal model accuracy is achieved with a maximum Courant number of about 0.25 and without a limitation upon θ_{\min} . Measured and computed stages with these parameter specifications are compared in Figure 20 at five locations on the tailwater. The stage measurement locations do not coincide exactly with the modeled sections, and proper interpretation of the offsets between measured and computed stage requires that these differences be considered. Overall agreement between the model and the data on wave timing, amplitude, and shape is excellent.

At the upstream-most gage (CRM 78.85) the model (CRM 78.7) reproduces all of the releases. An error in the chart speed of the stage recorder, beginning at hour 100, leads to an increasing timing discrepancy toward the end of the test. At the head of the long pool, CRM 76.1, wave timing and shape are well represented in the model CRM 76.2, but peak stages of the smaller-amplitude waves are slightly less attenuated than in the prototype. In the long pool, almost all roughness elements were submerged at low flow, and small values of Manning's roughness (0.015) were required to reproduce stage changes in the reach. At the downstream end of the pool, CRM 73.7, wave shapes, peaks, and timing are generally well represented in the model. Because the value of θ required for adequate diffusion in the model is small or negative, the smaller waves with short wavelengths are lagged, as projected in the linear analysis. Comparing the stage data at CRM 71.4 and 67.3 with the numerical simulation at CRM 71.2 and 67.2, respectively, also reveals excellent agreement. Again, due to negative θ values in the model, small, short-period waves arriving between hours 70 and 90 lag slightly in the simulation.

DISCUSSION AND CONCLUSIONS

Our linear analysis of the dynamic equations of open channel flow produced an equation describing wave advection, diffusion, and dispersion in rivers. In dimensionless form the equation provides insight regarding the importance of the various physical processes affecting the flow. The adequacy of the kinematic wave equation and the potential for shock formation in the channel are evaluated from the relative magnitude of the dimensionless diffusion coefficient. The analysis indicates that diffusion of short-period waves in rivers is an

important process and that wave celerity in natural rivers at small Froude numbers is dominated by friction and essentially independent of inertia.

We describe rapidly varying flow in tailwater streams with an inertia-free diffusion wave model. The model allows variable wave diffusion and does not require a downstream boundary condition. The modified-equation, Hirt, and von Neumann analyses of the model were conducted to improve accuracy and our interpretation of results. Identical stability conditions, developed with each approach, revealed that numerical stability does not impose a limitation upon the model time step or the minimum value of θ .

The Apalachia and Norris tailwater studies demonstrated that model behavior predictions of the linear analysis are valid for nonlinear cases. The dissipative and dispersive characteristics of the model are sensitive to the selection of spatial grid resolution, the Courant number, and θ . Guided by the analysis, spatial mesh resolution and maximum Courant number for optimal model accuracy can be estimated a priori, and the only calibration required for model application is the adjustment of Manning's roughness. The analysis showed that model damping increases as θ decreases, as the Courant number increases, and as wavelength relative to the spatial grid length Δx decreases. The model analysis also revealed

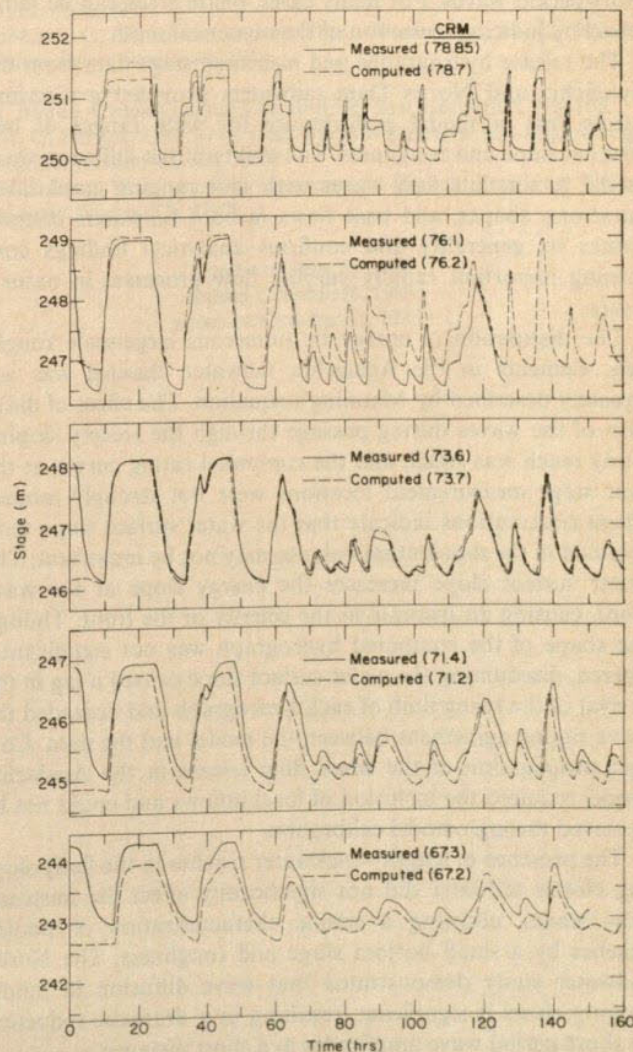


Fig. 20. Measured and computed stage at several locations on the Norris tailwater. A maximum Courant number of 0.25, spatial grid resolution of 800 m, and variable θ without a lower bound were conditions of the numerical simulation.

that damping and phase errors occur when the spatial grid is overly coarse in relation to wavelengths of interest. An accurate expression quantifying the numerical diffusion of the model was an important result of the modified equation analysis. The von Neumann and modified equation analyses of model phase error concurred and were supported over wide ranges of θ and the Courant number by linear routing studies; however, the frequently utilized Hirt analysis yielded incorrect phase relationships.

The capabilities and accuracy of the diffusion wave model are enhanced by allowing θ to vary so that a balance is maintained between physical and numerical diffusion. The limitation specified in many diffusion wave models—that the weighting parameter applied to the time derivative, in our case θ , be greater than 0.0—should not be generally applied. Mildly sloping rivers modeled with a fine spatial mesh for adequate wave resolution require negative values of this parameter for proper wave diffusion.

A physical/numerical dispersion balance eliminating model phase error cannot be maintained simultaneously with the diffusion balance. Leading phase errors, occurring as a result of light damping in the Apalachia tailwater model, were suppressed without adversely affecting the simulation. The phase lag introduced in the Norris tailwater simulation as a result of negative values of θ was minimal, noticeable only for small, short-period waves. For many cases, phase error can be minimized by judicious selection of the numerical mesh.

The release hydrographs and measured stage data from the Apalachia and Norris Dam tailwaters provided a discriminating test of model performance for wide ranges of bed channel slope and roughness. The ability of the diffusion wave model to simulate flow waves with wide ranging amplitudes, durations, shapes, and base flows in both tailwaters demonstrates its generality and confirms analytical findings concerning important rapidly varying flow processes in natural rivers.

The dissipation of energy by numerous large-scale roughness elements in the Apalachia tailwater channel was adequately described by Manning's equation. The effect of diffusion of the waves during passage through the steeply sloping study reach was small, and the computed rating curves at the four stage measurement locations were not strongly looped. These observations indicate that the water surface slope term retained in the momentum balance may not be important. The water surface slope increases the energy slope at the wave front, causing an increase in the celerity of the front. Though the shape of the computed hydrograph was not significantly altered, discounting the water surface slope caused a lag in the arrival of the rising limb of each hydrograph and degraded the wave timing agreement between the model and the data. Correct propagation of the small flow release in the Apalachia model required the inclusion of local inflows and could not be achieved through model calibration.

The presence of lengthy backwater reaches in the flatly sloping Norris tailwater did not significantly affect the unsteady flow waves, allowing a simple characterization of pooled reaches by a small bottom slope and roughness. The Norris tailwater study demonstrated that wave diffusion in mildly sloping rivers is significant, resulting in a dramatic reduction of short-period wave amplitudes in a short distance.

Dynamic waves of measurable size were not observed moving ahead of the main flow or propagating upstream as a result of wave reflection in either field study. Together with

these observations the reproduction of all features of the measured stage-time traces by the model demonstrates that rapidly varying flow in shallow rivers is not affected significantly by inertia. The dominance of friction over inertia for large wave propagation in deeper rivers was indicated by Stoker [1957] in his study of rapidly rising floods on the Ohio River. He reported that the first measurable disturbance traveled far behind the initial dynamic wave at the wave speed used in kinematic routing methods. As the importance of inertia is greatest for rapidly varying flow in a mildly sloped stream, we conclude that inertia is unimportant in natural, free-flowing rivers.

These results have clear implications for understanding the physical processes controlling downstream wave propagation following the breach of a dam. Frictional dissipation of large-amplitude flow waves is dominant over inertia and controls wave celerity. Because of the typical short-period nature of dam-break waves, diffusion affects wave amplitude significantly and acts to resist the formation of a shock front. Therefore, reliable prediction of wave amplitude and timing over distances greater than a few wavelengths depends upon accurate descriptions of these processes.

NOTATION

a	damping exponent, modified equation analysis.
A	cross-sectional area of the channel.
b	phase exponent, modified equation analysis.
B	channel width.
c	wave celerity.
\bar{c}	average wave celerity in a reach.
C	Chezy conveyance coefficient.
C_m	constant, Manning's equation.
C_r	Courant number.
D	diffusion coefficient.
D^*	dimensionless diffusion coefficient.
E	dispersion coefficient.
E_H	dispersion coefficient, Hirt analysis.
E^*	dimensionless dispersion coefficient.
F	Froude number.
g	acceleration due to gravity.
i	$\sqrt{-1}$.
j	spatial index.
k	wave number.
m	time index.
n	Manning's roughness coefficient.
$O(\)$	the order of.
q	discharge per unit width.
q_i	local inflow per unit length of channel.
Q	discharge.
\bar{Q}_k	amplitude of the discharge component of wave number k .
Q_0	discharge at previous time step.
Q^*	dimensionless discharge.
\dot{Q}	derivative of discharge with respect to time.
R	channel hydraulic radius.
r_k	complex amplification factor of the k th Fourier component.
S_f	slope of the energy grade line.
S_0	slope of the channel bottom.
t	time.
t^*	dimensionless time.
V	velocity.
x	distance.

- x^* dimensionless distance.
 y flow depth.
 y_0 flow depth at previous time step.
 $\Delta x, \Delta t$ finite distance and time increments.
 α grouping of parameters, diffusion wave model.
 β grouping of parameters, diffusion wave model.
 γ $k\Delta x$.
 θ balanced diffusion parameter.
 μ coefficients of terms in the modified equation.
 Φ_c phase angle of continuum solution.
 Φ_N phase angle of numerical solution.
 Φ_r ratio of numerical and continuum phase angles.
 $\langle \rangle$ average over time Δt .

Acknowledgments. The field investigations described in the paper were conducted and funded by the TVA Division of Water Resources. Initial model development and calibration were accomplished while M. Ferrick and J. Bilmes were with the TVA Water Systems Development Branch. We thank E. Wright of CRREL for reviewing the manuscript, W. Reid of TVA for developing the plot and data handling routines that were used extensively, and numerous other individuals in the TVA Division of Water Resources for assistance with and support of the field program.

REFERENCES

- Chang, C., E. D. Singer, and A. D. Koussis, On the mathematics of storage routing, *J. Hydrol.*, 61, 357-370, 1983.
 Cunge, J. A., On the subject of a flood propagation computation method (Muskingum method), *J. Hydraul. Res.*, 7(2), 205-230, 1969.
 Cunge, J. A., F. M. Holly, Jr., and A. Verwey, *Practical Aspects of Computational River Hydraulics*, pp. 357-360, Pitman, Marshfield, Mass., 1980.
 Dooge, J. C. I., W. G. Strupczewski, and J. J. Napiorkowski, Hydrodynamic derivation of storage parameters of the Muskingum Model, *J. Hydrol.*, 54, 371-387, 1982.
 Ferrick, M. G., Flow routing in tailwater streams, in *Computer and Physical Modeling in Hydraulic Engineering*, pp. 192-208, edited by G. Ashton, ASCE, New York, 1980.
 Henderson, F. M., Flood waves in prismatic channels, *J. Hydraul. Div. Am. Soc. Civil Eng.*, 89(HY4), 39-67, 1963.
 Koussis, A. D., An approximative dynamic flood routing method, paper presented at International Symposium on Unsteady Flow in Open Channels, BHRA Fluid Eng., Univ. Newcastle-upon-Tyne, England, April 12-15, 1976.
 Koussis, A. D., Comparison of Muskingum method difference schemes, *J. Hydraul. Div. Am. Soc. Civil Eng.*, 106(HY5), 925-929, 1980.
 Menéndez, A. N., and R. Norscini, Spectrum of shallow water waves: An analysis, *J. Hydraul. Div. Am. Soc. Civil Eng.*, 108(HY1), 75-94, 1982.
 Ponce, V. M., and D. B. Simons, Shallow wave propagation in open channel flow, *J. Hydraul. Div. Am. Soc. Civil Eng.*, 103(HY12), 1461-1476, 1977.
 Ponce, V. M., R. M. Li, and D. B. Simons, Applicability of kinematic and diffusion models, *J. Hydraul. Div. Am. Soc. Civil Eng.*, 104(HY3), 353-360, 1978.
 Richtmyer, R. D., *Difference Methods for Initial Value Problems*, pp. 49-73, Interscience, New York, 1957.
 Roache, P. J., *Computational Fluid Dynamics*, pp. 36-48, Hermosa, Albuquerque, N. M., 1976.
 Smith, A. A., A generalized approach to kinematic flood routing, *J. Hydrol.*, 45, 71-89, 1980.
 Stoker, J. J., *Water Waves*, pp. 482-509, Interscience, New York, 1957.
 Strupczewski, W., and Z. Kundzewicz, Muskingum method revisited, *J. Hydrol.*, 48, 327-342, 1980.
 Warming, R. F., and B. J. Hyett, The modified equation approach to the stability and accuracy analysis of finite-difference methods, *J. Comput. Phys.*, 14, 159-179, 1974.
 Weinmann, P. E., and E. M. Laursen, Approximate flood routing methods: A review, *J. Hydraul. Div. Am. Soc. Civil Eng.*, 105(HY12), 1521-1536, 1979.
 Whitham, G. B., *Linear and Nonlinear Waves*, pp. 19-42, Wiley-Interscience, New York, 1974.
 J. Bilmes, General Digital Corporation, East Hartford, CT 06108.
 M. G. Ferrick, U.S. Army Cold Regions Research and Engineering Laboratory, Hanover, NH 03755.
 S. E. Long, Water Systems Development Branch, Tennessee Valley Authority, Norris, TN 37828.

(Received June 3, 1983;
 revised October 28, 1983;
 accepted October 31, 1983.)